表　　題　喫煙は血管平滑筋細胞での新規細胞死フェロトーシスを誘導し、大動脈瘤形成に寄与する

論 文 の 区 分　博士課程

著　　者　　名　サンピルワンジル　アリウナー

担当指導教員氏名　高橋　将文　教授

所　　属　自治医科大学大学院医学研究科
専攻　地域医療学系
専攻分野　血液・免疫疾患学
専攻科　炎症免疫学

2021 年 02 月 19 日申請の学位論文

Contents of the Dissertation

Abbreviations

AA – Aortic aneurysm

AD – Aortic dissection

AAA – Abdominal aortic aneurysm

ACR – Acrolein

CPO – 2-cyclopentene-1-one

CSE – Cigarette smoking extract

DPI – Diphenyleneiodonium chloride

DFO – Deferoxamine

DMSO – Dimethyl sulfoxide

ECM – Extracellular matrix

EVG – Elastic Van Gieson

Fer-1 – Ferrostatin-1

GSH – Glutathione

GSSG – Glutathione disulfide

GPX4 – Glutathione peroxidase 4

HMGB1 – High mobility group box 1

4-HNE – 4-hydroxyl-2-nonenal

IL-1β – Interleukin-1 beta

IL-6 – Interleukin-6

Lip-1 – Liproxstatin-1

LDH – Lactate dehydrogenase

LOX – Lipoxygenase

MVK – Methyl vinyl ketone

Nec-1 – Necrostatin-1

NAC – N-acetyl cysteine

Ptgs2 – Prostaglandin-endoperoxide synthase 2

PBS – Phosphate-buffered saline

ROS – Reactive oxygen species

TAA – Thoracic aortic aneurysm

TNF-α – Tumor necrosis factor-alpha

TIMP-1 – Tissue inhibitor of metalloproteinases-1

TEM – Transmission electron microscopy

VSMC – Vascular smooth muscle cell

1. Introduction

Aortic aneurysm (AA) is a common problem with life-threatening consequences, which is characterized by permanent and irreversible dilatation of the aorta with an enlargement of 50 percent greater than the normal size [1]. AA most often affects the older males and is the 15th leading cause of death in the United States, resulting in over 15,000 deaths per year [2]. In most AA cases, patients do not have symptoms until the disease is at an advanced stage. The lack of aneurysm specific symptoms often renders them unnoticed until the aorta ruptures, resulting in significant morbidity and mortality.

Once ruptured, excessive intra-abdominal hemorrhage will require emergency surgery and is associated with an increased risk of morbidities due to delays in transportation and diagnosis. Despite the prompt diagnosis and early surgery, the mortality rate from ruptured AA has not decreased significantly. Furthermore, despite many advances in medicine, such as anesthesia, emergency care, and surgical treatment, AA mortality rates have not been improved significantly in recent decades. Thus, improvement in emergency care during AA rupture is unlikely to significantly impact the survival rate from this fatal condition, suggesting that advances in medical technology will not play a significant role in reducing mortality unless there is a substantial therapeutic advance in treatment. The lack of non-invasive interventional treatment in these patients suggests that a better understanding of the disease pathophysiology is needed to implement new treatment strategies.

The aorta functions to efficiently transmitting pulsatile arterial blood pressure to the whole arterial tree, which depends primarily on its structural properties, such as vascular smooth muscle cells (VSMCs), elastin, and collagen. The aortic wall is composed of a three-layered structure [3]: the intima, the media, and the adventitia. The media is the thickest layer that contains the basic structural and functional unit of the aorta known as the lamellar unit [4]. Each lamellar unit comprises a layer of VSMCs

sandwiched between two layers of elastic fibers. This unit has both tensile strength and elastic recoil properties, allowing the aorta to withstand high pressures and return to its initial diameter during diastole.

The layers of the aorta histologically change in different manners during the remodeling response. As the aorta expands, the adventitia thickens and becomes highly populated with inflammatory cells [5]. Collagen deposition occurs in the adventitia and media at the early stage of the aneurysm, whereas collagen degradation occurs at the end-stage [6]. The media appears hypertrophic with VSMC depletion and medial neovascularization [7-8]. The elastic lamellae appear degenerated and disconnected [9].

Although some AAs have specific causes, such as trauma or infection, the vast majority is associated with various risk factors. Chronic smokers are four times more likely to develop AA than non-smokers [11-12]. Advanced age is a major risk factor for AA, which begins to appear in people aged 55 and is present in 10 percent of 80-year-olds [13]. Atherosclerosis, hypertension, and lower extremity disease are also considered to be risk factors [14-16].

AA can occur both in the thoracic and abdominal parts of the aorta, depending on its localization. Thoracic AA (TAA) is mostly accompanied by genetically inherited conditions, such as Ehlers-Danlos syndrome, Marfan syndrome, and Loeys-Dietz syndrome [17]. On the other hand, abdominal AA (AAA) does not typically demonstrate such an inheritance. Pathologically, however, they share several common features.

Current evidence on AA's pathogenesis suggests several critical players involved in the initiation and progression of AA: elastic fiber degradation, aortic wall inflammation, and VSMC loss [18]. The leading underlying cause of AA formation is the breakdown of elastin and collagen in the aortic media. This process is associated with inflammatory processes, activation of proteases, cytokine secretion [19-21], and

phenotypic modulation of VSMCs [22]. As inflammatory cells migrate into the aortic wall, they release chemokines and cytokines, which cause further migration of leukocytes into the aortic wall, and results in the activation and expression of matrix metalloproteinases (MMPs). Four members of the MMP family degrade insoluble elastin fibers effectively *in vitro*, including the MMP-2, MMP-9, matrilysin (also known as MMP-7), and macrophage elastase (MMP-12). All of these enzymes have been detected in human AA samples. Additional evidence indicates that other MMPs are likely responsible for aortic wall collagen degradation, such as interstitial collagenase-1 (also known as MMP-1) and collagenase-3 (also known as MMP-13). In AAA tissues, MMPs (MMP-1, -2, -3, -7, -9, -12, and 13), serine proteases, and cysteine proteases are all detected at higher concentrations than those occurs in normal or stenotic atherosclerotic arteries. MMP-2 and MMP-9 are the most frequently detected proteolytic species in developing and established AA. MMP-2 activation within the aneurysm has been associated with initial development [23]. On the other hand, expression of MMP-9 has been demonstrated to be correlated with increased aneurysm diameter on AA. In addition, increased expression levels of tissue inhibitor of metalloproteinases-1 (TIMP-1) are highly correlated to medium-large human AAs, but not to the small AAs. Concomitantly, plasma MMP-9 and TIMP-1 levels are also significantly higher in patients with AA than those in patients with aortic occlusive disease or in healthy volunteers [24-25].

VSMCs are major cell types that are abundantly present in the aortic wall's media and a vital component in the typical arterial structure. They involve the synthesis of elastin, collagen, and other extracellular matrix components [10]. In typical aneurysmal arteries, VSMC loss is a prominent phenomenon, though it is unknown whether or not cell death is an active pathological event or a consequence of tissue deterioration. The importance of medial VSMC loss in AA development had been evidenced by previous

studies showing that inhibitors of major forms of regulated cell death, such as apoptosis and necroptosis, prevented AA formation through stabilizing VSMCs and suppressing inflammation [26-27].

Overall, the above-mentioned mechanistic events cause the dilation of the aorta by destroying the medial layer. As the vessel wall dilates, the stress experienced by the vessel causes further dilation and may eventually lead to rupture. However, the exact causative mechanistic chain reactions involved in AA formation are unclear. It is believed to be caused by a complex interaction among the aortic wall's structural properties and various risk factors such as atherosclerosis, cigarette smoking, arterial hypertension, aging, and sex. In particular, epidemiologic studies have underlined the strong impact of smoking on the incidence, progression, and rupture risk of AA. Cigarette smoke induces damage to the arterial wall, and excess risk for AA formation remained four times greater in the current smokers than that of never smokers [28]. It is also considered that smoking is responsible for 75% of the excess prevalence of aneurysms greater than 4 cm. Indeed, current smoking is likely to increase the risk of perioperative death in patients with AA [29]. However, the mechanisms by which cigarette smoke induces these effects are still not precise.

Cigarette smoke is a highly dynamic complex mixture of chemical compounds, known to contain thousands of chemicals [30]. These chemical compounds are differentially distributed in the tar (particulate) phase and the gas phase, and their impacts on smokers' health differ [31]. First, the tar phase regroups the particles with a size greater than 0.1 µm, contains nicotine, tar, tobacco specific-nitrosamines, and polynuclear aromatic hydrocarbons. Second, the gas-phase contains smaller particles with less than 0.1 µm, passing through the airway epithelial barrier to enter the circulation to induce the systemic effects [32]. Separation of gas-phase from tar requires continuous sucking of cigarette smoke through a Cambridge filter, followed by

bubbling it into phosphate-buffered saline (PBS) [33]. This tar and nicotine-free gas-phase are called cigarette smoking extract (CSE), which consists of carbon monoxide, reactive oxygen species (ROS), and various carbonyl compounds [32], and passes through the airway epithelial barrier increase the systemic oxidative stress and oxidative damage [33], contributing to the development of AA.

Multiple studies have shown that cigarette smoke-related adverse effects are related to intracellular organelle damage, ROS formation, and inflammation. Indeed, previous investigations have demonstrated that CSE induces various cytotoxic effects in a wide range of cell types. The mechanism of CSE-induced cytotoxicity is thought to incorporate oxidative stress, leading to oxidative damage and apoptotic cell death [31, 34]. Although apoptosis has been considered to be the primary mechanism involved in CSE-induced cytotoxicity, observations regarding the absence of cleaved caspase-3 and pan-caspase inhibitor Z-VAD's ineffectiveness had questioned the presence of apoptosis in CSE-induced cytotoxicity [35]. Thus, the molecular mechanism of CSE-induced cytotoxicity remains to be elucidated.

Glutathione (GSH) is the thiol-dependent antioxidant system and the prepared substrate for glutathione peroxidase 4 (GPX4) and plays a crucial role in the cellular redox balance [36]. The gaseous phase of the cigarette smoke is highly reactive, resulting in GSH exhaustion both *in vitro* and *in vivo* settings. Moreover, GSH supplementation was shown to rescue cells from CSE-induced death, indicating that GSH depletion is a critical phenomenon in the progression of CSE-induced cellular cytotoxicity and suggesting the involvement of GSH in the cigarette smoke detoxification.

A newly regulated cell death form called ferroptosis was discovered in 2012 by Stockwell's group [37]. Ferroptosis is an iron-dependent form of cell death characterized by an accumulation of polyunsaturated phospholipid hydroperoxides at

the cellular plasma membrane in the presence of ferrous ions. Mechanistically, ferroptosis initially occurs through the inhibition of GPX4 directly or indirectly through the loss of intracellular GSH content [38-39].(Figure 1.)

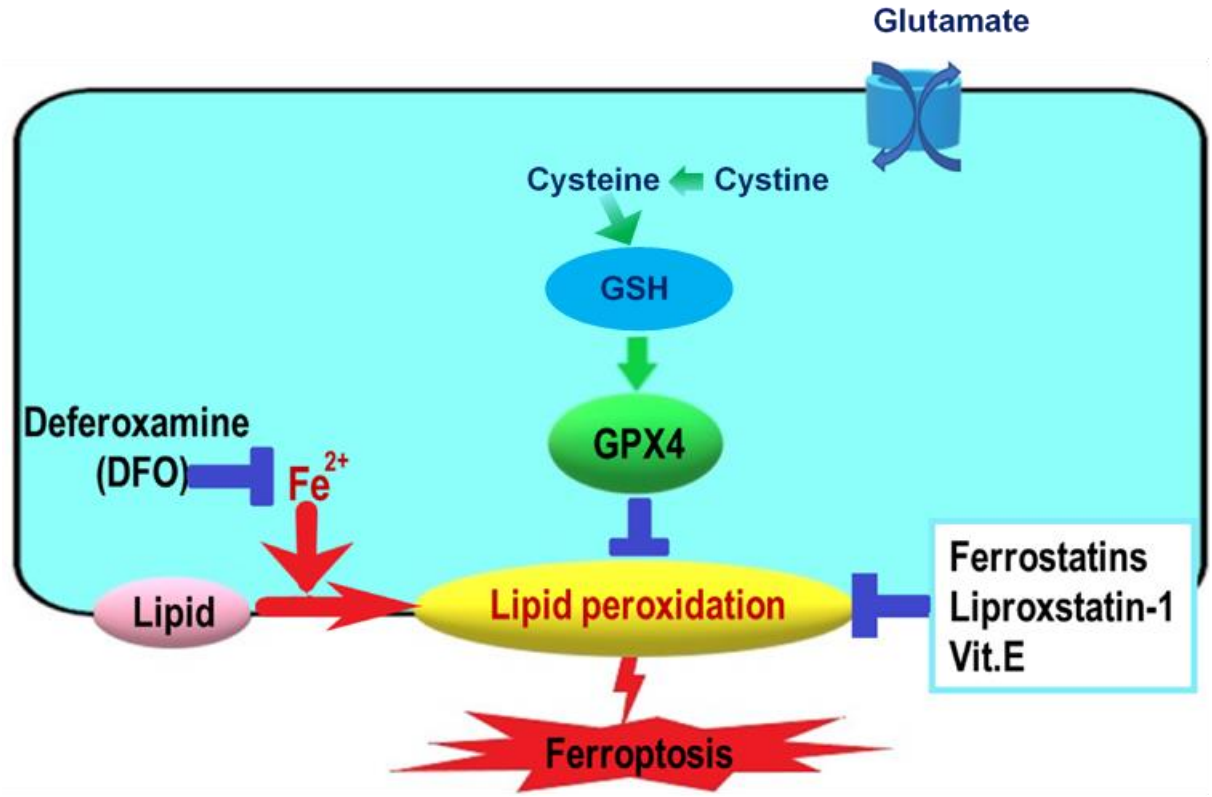

Figure 1. Classical mechanism of ferroptosis

Loss of GPX4 activity directly or indirectly through GSH depletion triggers accumulation of lipid peroxides, which finally results ferroptosis. Ferrostatin-1 (Fer-1) and Liproxstatin-1 (Lip-1) are specific inhibitors of ferroptosis, and vitamin E (Vit.E) and iron chelators known to suppress ferroptosis.

The involvement of ferroptosis in certain pathological conditions had been elucidated [40-41]. A very recent study showed that ferroptosis is involved in cigarette smoking-induced chronic obstructive pulmonary disease [42]. However, it is unclear whether or not CSE is involved in VSMC cytotoxicity and AA formation. The purpose of this study is to analyze the relationship between cigarette smoking and AA formation. Because the GSH depletion is the starting point of CSE-induced cytotoxicity, it is inferred that ferroptosis might contribute to this process.

2. Materials and methods

2-1. Cell culture and reagents

Primary cultures of VSMCs were obtained from the media of aortas of male Sprague-Dawley rats by digestion with trypsin and collagenase, as described previously [43]. A7r5 (rat VSMC) and EAhy926 (human endothelial cell) lines were obtained from ATCC (Manassas, VA). 10T1/2 cells (mouse fibroblasts) were obtained from RIKEN BioResource Center (Tsukuba, Japan). The cells were cultured in Dulbecco's modified Eagle's medium (DMEM, Wako, Osaka, Japan) containing 10% fetal calf serum (FCS, Dainippon Pharmaceutical Company, Osaka, Japan). Primary VSMCs with 4–6 passages were used for the experiments.

CSE was prepared as previously described [31]. Briefly, cigarettes (17 mg tar/cigarette; Hi-Lite, JT Tokyo, Japan) were combusted, and the mainstream of the cigarette smoke was continuously sucked through a standard glass-fiber Cambridge filter at a constant flow rate of 1.050 L/min by an aspiration pump to remove the tar phase and nicotine. The remaining gas phase of cigarette smoke was bubbled into 15 mL of PBS. After cigarette combustion, the Cambridge filter was dried in air at 25°C for 12 h, and the increase in the dry weight of the filter was regarded as the amount of the tar phase. The concentration of CSE was expressed in terms of the virtual tar concentration, which was calculated on the assumption that the tar trapped on the Cambridge filter is dissolved in the PBS used for CSE preparation. The CSE preparations were aliquoted and stored at –80°C until use.

Ferrostatin-1 (Fer-1), Liproxstatin-1 (Lip-1), and diphenyleneiodonium chloride (DPI) were purchased from Cayman Chemical (Ann Arbor, MI). Deferoxamine (DFO) was purchased from Abcam (Cambridge, MA). Acrolein (ACR), methyl vinyl ketone (MVK), and 2-cyclopentene-1-one (CPO) were purchased from Tokyo Chemical Industry (Tokyo, Japan). RSL3 was purchased from AdooQ

Bioscience (Irvine, CA). Z-VAD-FMK, Z-YVAD-FMK, and Necrostatin-1 (Nec-1) were purchased from MBL (Nagoya, Japan), Biovision Incorporated (Milpitas, CA), and Santa Cruz (Dallas, TX), respectively. N-acetyl cysteine (NAC) was purchased from Wako Pure Chemical Industries (Osaka, Japan). Fer-1, Lip-1, DPI, and RSL-3 were dissolved in dimethyl sulfoxide (DMSO). MVK, ACR, and CPO were dissolved in PBS. Other reagents were obtained from Sigma-Aldrich (St. Louis, MO) unless otherwise specified.

2-2. Cell death assay

Cell death was assessed with SYTOX Green (Thermo Fisher Scientific), a membrane-impermeable DNA dye that enters dead cells. Nuclei were co-stained with Hoechst33342 (Dojindo, Kumamoto, Japan). Fluorescence intensity was measured by using a multimode microplate reader (Spark, TECAN, Switzerland). Cytotoxicity was determined as lactate dehydrogenase (LDH) activity using a cytotoxicity detection kit (Roche, Mannheim, Germany) according to the manufacturer's instructions.

2-3. Assessment of lipid peroxidation

Lipid peroxidation was assessed by the fluorescent dye C11-BODIPY$^{581/591}$ (Thermo Fisher Scientific). Briefly, cells were cultured overnight and labeled with 5 μM C11-BODIPY$^{581/591}$ in 0.1% BSA/DMEM for 1 h before CSE treatment. Fluorescence intensity was measured after the addition of CSE at 10-min intervals by using a multimode microplate reader (Spark, TECAN). Nuclei were labeled with Hoechst33342. Representative images were obtained at 1 h after CSE treatment using an FV10i confocal laser scanning microscope (Olympus, Tokyo).

2-4. Real-time RT-PCR

Total RNA was extracted from the cells using ISOGEN (Nippon Gene Co., Ltd., Toyama, Japan), according to the manufacturer's instructions. Real-time RT-PCR

analysis was performed using the Takara TP960 PCR Thermal Cycler Dice Real-Time System II (Takara Bio Inc., Shiga, Japan) for the measurements of mRNA expression. Primer sequences are shown in Table.1.

Table.1 Primer sequences used in Real-Time PCR

Gene	**Forward**	**Reverse**
Tnfα	5'-ATGGGCTCCCTCTCATCAGT-3'	5'-ACTCCAGCTGCTCCTCTGCT-3'
Il1b	5'-CACCTCTCAAGCAGAGCACAG-3'	5'-GGGTTCCATGGTGAAGTCAAC-3'
Il6	5'-TCCACCCCCAACTTCCAATGCTC-3'	5'-TTGGATGGTCTTGGTCCTTAGCC-3'
Ptgs2	5'-TCCTCCTGTGGCTGATGACT-3'	5'-CGGGATGAACTCTCTCCTCA-3'
Mmp2	5'-ACCGTCGCCCATCATCAA-3'	5'- TTGCACTGCCAACTCTTTGTCT-3'
Mmp9	5'-TCGAAGGCGACCTCAAGTG-3'	5'-TTCGGTGTAGCTTTGGATCCA-3'
Timp1	5'-CGCAGCGAGGAGGTTTCTCAT-3'	5'-GGCAGTGATGTGCAAATTTCC-3'
Gapdh	5'-AACGGCACAGTCAAGGCTGA-3'	5'-ACGCCAGTAGACTCCACGACAT-3'

Gene expression was normalized to GAPDH expression using the software provided with the system. Because cytotoxicity was observed in the cells treated with CSE for 4 h, we evaluated the quality and yield of RNA and confirmed that isolated RNA could be used for assessing mRNA expression. The quality of RNA is shown in Table.2

Table.2 Quality of RNA in CSE-treated A7r5 cells

Sample Id	**Nucleic Acid Conc.**	**Unit**	**A260**	**A280**	**260/280**	**260/230**
Cont-1	471.6	ng/μL	11.79	6.05	1.95	1.83
Cont-2	440.4	ng/μL	11.01	5.91	1.86	1.97
Cont-3	424.6	ng/μL	10.61	5.61	1.89	1.84
3 h CSE-1	306.4	ng/μL	07.66	3.99	1.92	1.93
3 h CSE-2	311.4	ng/μL	07.78	4.01	1.94	1.87
3 h CSE-3	259.3	ng/μL	06.48	3.29	1.97	1.78
4 h CSE-1	257.0	ng/μL	06.42	3.45	1.86	1.96
4 h CSE-2	274.7	ng/μL	06.86	3.58	1.91	1.91
4 h CSE-3	246.3	ng/μL	06.16	3.28	1.88	1.88

2-5. GSH measurement

Total GSH and glutathione disulfide (oxidized glutathione, GSSG) were evaluated by a GSSG/GSH Quantification Kit (Dojindo, Kumamoto, Japan) according to the manufacturer's instructions. The amount of reduced GSH (shown as GSH) was calculated as total GSH – 2GSSG, and the ratio of GSH to GSSG was shown.

2-6. Establishment of GPX4-expressing A7r5 cells

Mouse GPX4 sequence including SECIS element was amplified with the primer pair forward, 5′- ACCATGTGTGCATCCCG-3′; reverse, 5′- AGGCAGCCAGGGTGAAG-3′ and subcloned into the CS-CA-MCS plasmid (kindly provided by Dr. H. Miyoshi, RIKEN BioResource Center) [45]. To produce a lentiviral vector, LentiX293T cells (Takara Bio) were transfected with CS-CA-MCS, pLP1, pLP2, and pVSVG using PEI MAX (Polysciences, Warrington, PA). Culture media containing the lentiviral vectors were collected 3 days after transfection. The collected media were filtered with a 0.45-μm filter and ultracentrifuged at 21,000 rpm for 2 h using a Type 45 Ti rotor (Beckman Coulter, Brea, CA). The pellets were then suspended again in 5% FCS/PBS. The lentiviral titer was measured using a Lentivirus qPCR Titer kit (Applied Biological Materials, Richmond BC, Canada). To transduce the lentiviral vectors, A7r5 cells were incubated with 8 μg/mL of polybrene. Humanized Kusabira-Orange1 (hKO1) subcloned into CS-CA-MCS was used as a negative control.

2-7. Western blot analysis

Western blotting was performed using primary antibodies for GPX4 (Santa Cruz Biotechnology, Dallas, TX), caspase-3 (No.9665, Cell Signaling Technology, Boston, MA), and β-actin (No.A5441; Sigma-Aldrich). Briefly, proteins were separated by denaturing discontinuous SDS-polyacrylamide gel electrophoresis, under reducing conditions, according to Laemmli's (1970) method. All gels were prepared from a 30%

stock of pre-weighed, pre-mixed acrylamide/bis-acrylamide solution. Samples containing 20 μg of total protein were mixed with a one-fifth volume of 5x, Reducing Loading Buffer, and boiled at 95 °C for 5 min. The samples were cooled down and then spin down briefly before loading. Each gels were run at a constant voltage of 20 mA until the dye front reaches the bottom of the gel (approximately 1.5 h). The gel was removed from the cast, the stacking gel was cut off, and went through the transfer process using a semidry transfer system at a constant current (500 mA) for 25 min. Next, the transfer apparatus disassembled, and the nitrocellulose membrane was placed in a container and rinsed twice for 5 min each with tris-buffered saline containing 0.1% Tween 20 (TBS-T). The membranes were blocked for 1 h in blocking buffer at room temperature before overnight incubation with primary antibodies at 4 °C. Next, the blots were washed with TBS-T and then incubated with appropriate horseradish peroxidase-conjugated secondary antibodies for 1 h at room temperature. Immunoreactive bands were visualized by Western BLoT Quant HRP Substrate (Takara Bio). The expression levels of β-actin served as an internal control for protein loading.

2-8. Animal experiments

All animal experiments were approved by the Use and Care of Experimental Animals Committee of Jichi Medical University (permit number 17151), and carried out in accordance with Jichi Medical University guidelines. C57BL/6J wild-type mice (8-10 weeks old, male) were purchased from Japan SLC, Inc. (Tokyo, Japan). Mice were housed (4/cage, RAIR HD ventilated Micro-Isolator Animal Housing Systems, Lab Products, Seaford, DE) in an environment maintained at 23 ± 2˚C with *ad libitum* access to food and water under a 12-h light and dark cycle with lights on from 8:00 to 20:00. The aorta was harvested immediately after the mice were sacrificed, washed in 0.1% antibiotics/PBS, and it was cut into 3–4 mm rings. The aortic rings were cultured

in 10%FCS/DMEM for 3 h, and then treated with CSE (0.8 mg/mL) for the indicated periods.

2-9. Histology and immunohistochemistry

The aortic rings were embedded and frozen in Tissue-Tek O.C.T. compound (Sakura Finetechnical Co. Ltd., Tokyo, Japan), and were cut into 10 μm-thick sections using a cryostat (Leica CM1850; Leica Microsystems, Germany). The sections were stained with elastic van Gieson (EVG). Dead cells in the aortic rings were detected by using SYTOX Orange staining (Thermo Fisher Scientific). SYTOX Orange was added to the culture media for 3 h before the harvest of the aortic rings. For quantitative analysis, two aortic rings from each of three mice were used. Immunohistochemical analysis was performed using antibody against the lipid peroxidation marker 4-hydroxyl-2-noneal (4-HNE; clone HNEJ-2; Japan Institute for the Control of Aging, Nikken SEIL, Shizuoka, Japan). The images of stained sections were digitized and analyzed by using a microscope (FSX-100; Olympus) or a confocal laser-scanning microscope (FV-10i, Olympus). The elastic fiber and non-elastic areas in the media were quantified using Image J software (National Institutes of Health, Bethesda, MD).

2-10. Transmission electron microscopy (TEM)

CSE-treated aortic rings were washed with PBS, fixed with buffered 2.5% glutaraldehyde and 4% paraformaldehyde for 2 h, and then washed with 0.1M phosphate buffer (pH 7.2) containing 4% sucrose. Post-fixation was performed with 1% OsO_4 solution in 0.1M phosphate buffer (pH7.4) for 90 min, and dehydration followed by infiltration of propylene oxide was performed. The samples were infiltrated with epoxy resins, and the resin was polymerized at 60°C for 72 h. Ultra-thin sectioning was

done at a thickness of 70–80 nm, and the sections were stained by a double-contrast method using 2% uranyl acetate and Reynolds lead citrate solution. The sections were observed under a transmission electron microscope (H-7700, Hitachi High-Technologies, Tokyo, Japan).

2-11. Statistical analysis

Data are expressed as the mean ± standard error of the mean (SEM). The Mann–Whitney test was used to compare two groups. Differences between multiple group means were determined by one-way ANOVA combined with the Tukey test or two-way ANOVA with Bonferroni post-hoc test. All analyses were performed using Prism (GraphPad Software, La Jolla, CA). A *p*-value of < 0.05 was considered statistically significant.

3. Results

3-1. Effect of CSE on cell death in vascular cells

We first examined the effect of CSE treatment on cell death in vascular wall cells by using SYTOX Green and LDH release assays and found that CSE treatment (0.2–0.8 mg/mL) induced cell death in A7r5 cells in a time- and dose-dependent manner (Fig. 2A and B).

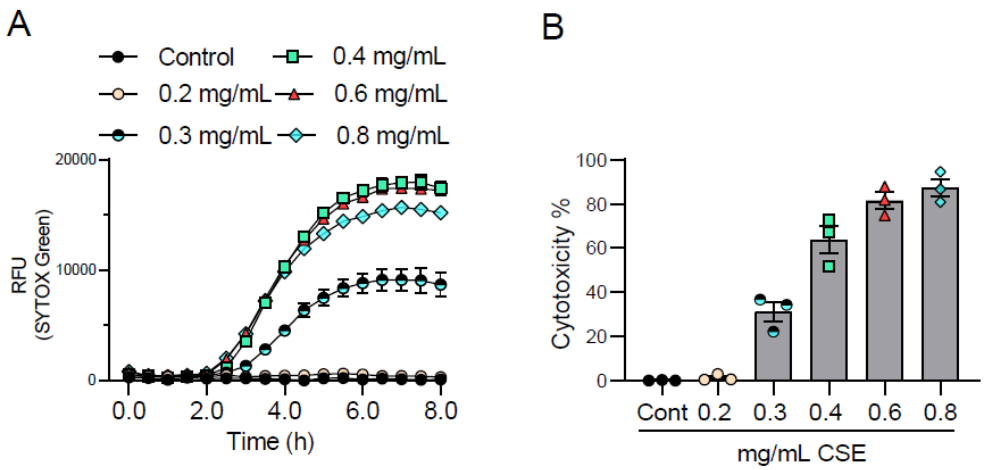

Figure 2. Dose-dependent effect of CSE on cell death

A7r5 cells were treated with CSE at the indicated concentrations. (A) Cell death was assessed with SYTOX Green, and the fluorescence intensity was measured at 30 min intervals (n = 3). (B) Cytotoxicity at 4 h after CSE treatment was assessed by an LDH release assay (n = 3). Data are expressed as the mean ± SEM.

We also confirmed that the CSE-induced cell death was entirely inhibited by ferroptosis specific inhibitors Fer-1 (5 μM) and Lip-1 (1 μM) (Fig. 3A, B and C). RSL-3 was used as a positive control to induce ferroptosis, and as expected, RSL3-induced cell death was entirely inhibited by Fer-1.

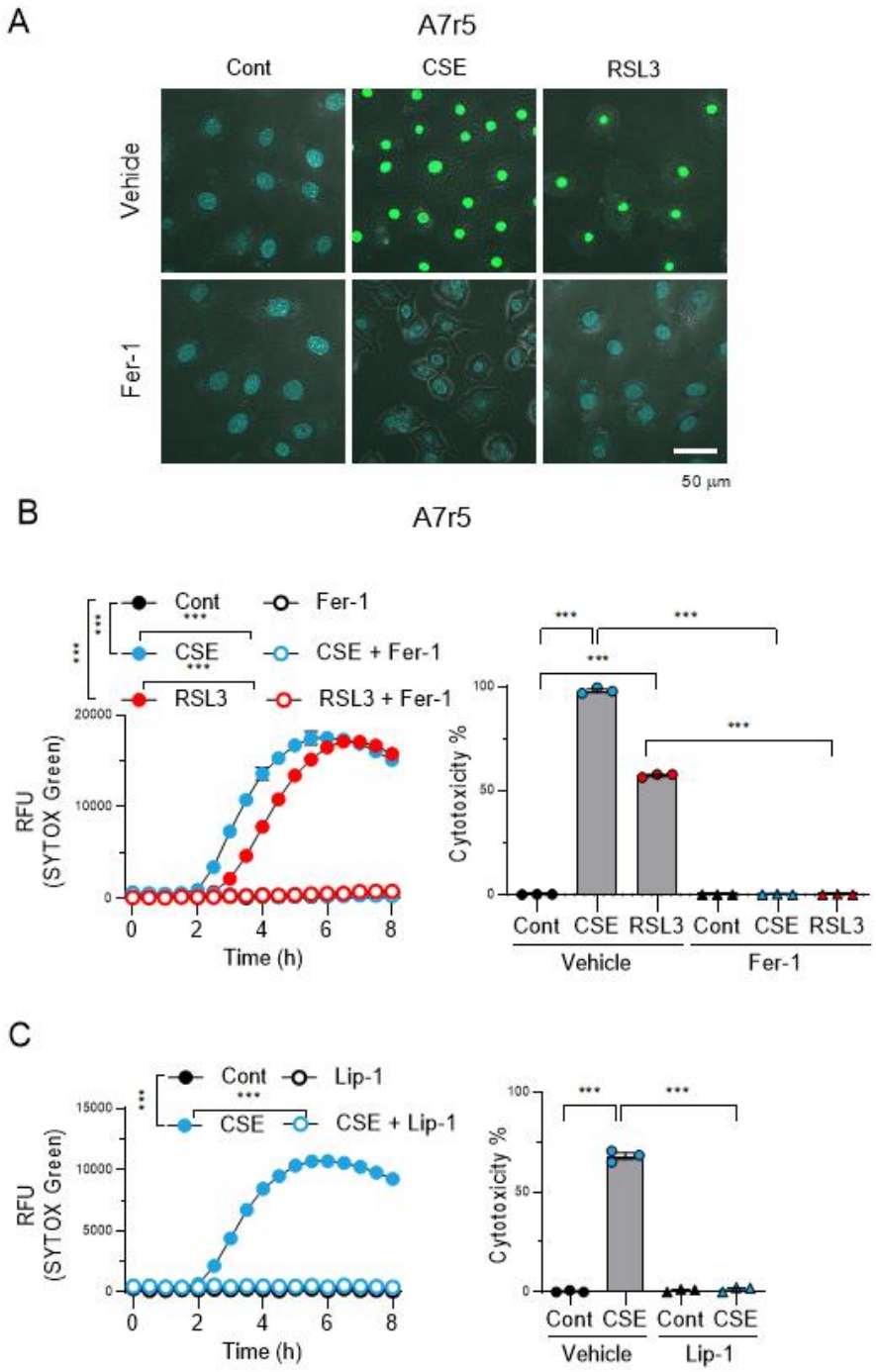

Figure 3. Effect of CSE on cell death in A7r5 cells

(A and B) A7r5 cells were treated with CSE (0.8 mg/mL) or RSL-3 (3 μM) in the presence or absence of Fer-1 (5 μM). (A) Representative images of SYTOX Green staining. (B) Cell death was assessed with SYTOX Green, and the fluorescence intensity was measured at 30-min intervals (n = 3). Cytotoxicity at 4 h after CSE treatment was assessed by an LDH release assay (n = 3). (C) A7r5 cells were treated with CSE (0.8 mg/mL) in the presence or absence of Lip-1 (1 μM). Cell death and cytotoxicity were assessed with SYTOX Green and by an LDH release assay, respectively. Data are expressed as the mean ± SEM. ***$p < 0.001$.

Consistent with this finding, CSE treatment induced cell death in primary rat VSMCs with a time course similar to that with A7r5 cells, and this cell death was completely inhibited by Fer-1 (Fig. 4A, B).

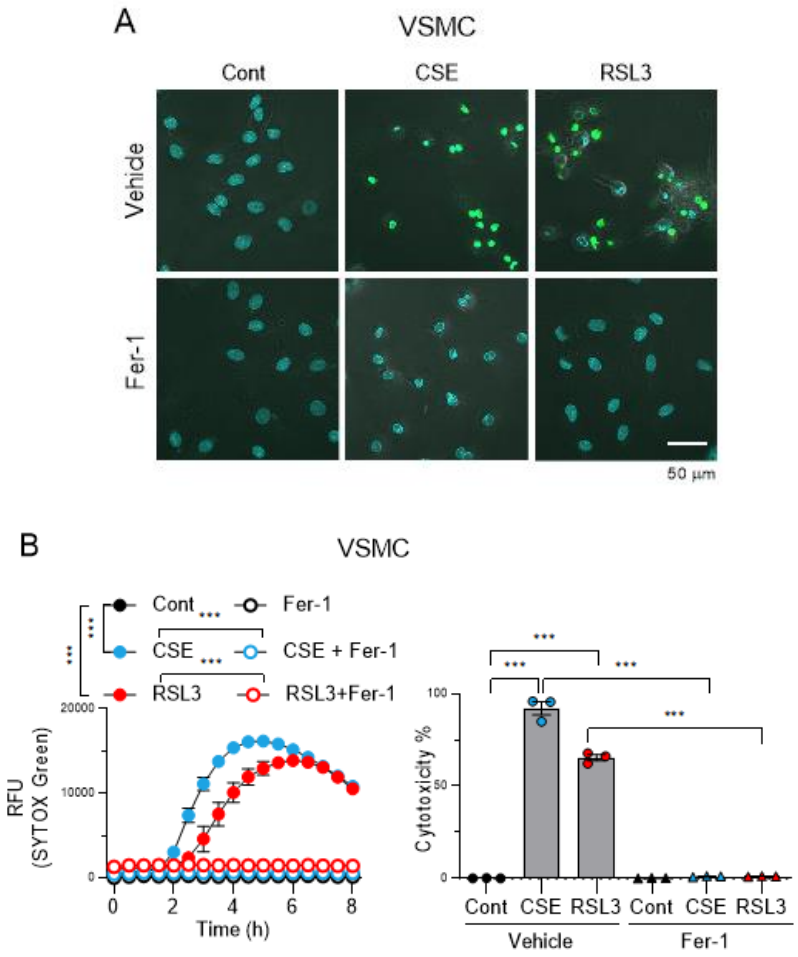

Figure 4. Effect of CSE on cell death in primary VSMCs

(A and B) Primary VSMCs were treated with CSE or RSL-3 in the presence or absence of Fer-1. (A) Representative images of SYTOX Green staining. (B) Cell death and cytotoxicity were assessed with SYTOX Green and by an LDH release assay, respectively (n = 3). Data are expressed as the mean ± SEM. ***$p < 0.001$.

We examined the effect of CSE treatment on cell death in EAhy926 endothelial cells and 10T1/2 fibroblasts regarding other types of vascular wall cells. While CSE treatment did not affect EAhy926 cells, it modestly induced cell death in 10T1/2 fibroblasts, which was inhibited by Fer-1 (Fig. 5A, B).

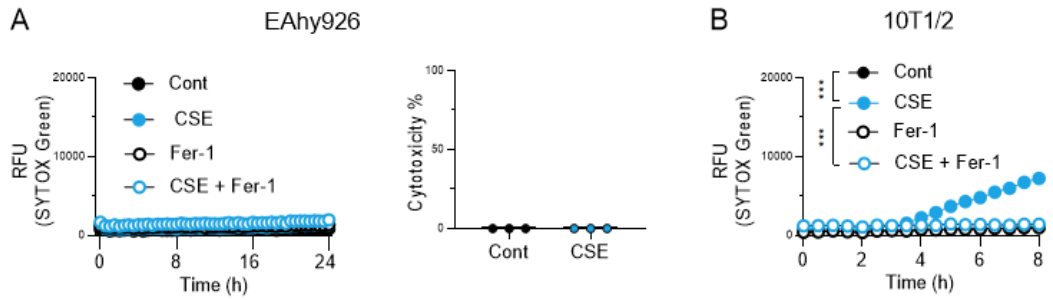

Figure 5. Effect of CSE on cell death in vascular endothelial cells and fibroblasts

(A) EAhy926 cells were treated with CSE in the presence or absence of Fer-1. Cell death and cytotoxicity were assessed with SYTOX Green and by an LDH release assay, respectively (n = 3). (B) 10T2/1 cells were treated with CSE in the presence or absence of Fer-1. Cell death was assessed with SYTOX Green. Data are expressed as the mean ± SEM. ***$p < 0.001$.

These findings suggest that, among vascular wall cells, VSMCs are the most sensitive to CSE-induced cytotoxicity, which is inhibited by specific inhibitors of ferroptosis.

3-2. CSE-induced ferroptosis, inflammatory responses, and matrix degradation in VSMCs

To rule out the possibility that other types of cell death, such as apoptosis, necroptosis, and pyroptosis, are involved in CSE-induced VSMC death, we next examined the effects of various inhibitors of these cell death pathways. Again, CSE markedly induced VSMC death in both A7r5 cells and primary VSMCs, and CSE-induced cell death was entirely abolished by Fer-1 and DFO (iron chelator) and partially abolished by NAC (GSH precursor) and DPI (NADPH oxidase inhibitor) (Fig. 6A and B). In contrast, CSE-induced cell death was not affected by Z-VAD (pan-caspase inhibitor [apoptosis inhibitor]), Z-YVAD (caspase-1 inhibitor [pyroptosis inhibitor]), or Nec-1 (necroptosis inhibitor), indicating that ferroptosis is the mechanism responsible

for CSE-induced VSMC death. Consistent with this result, cleaved caspase-3 was not detected in A7r5 cells treated with CSE in the presence or absence of Fer-1 (Fig. 6C).

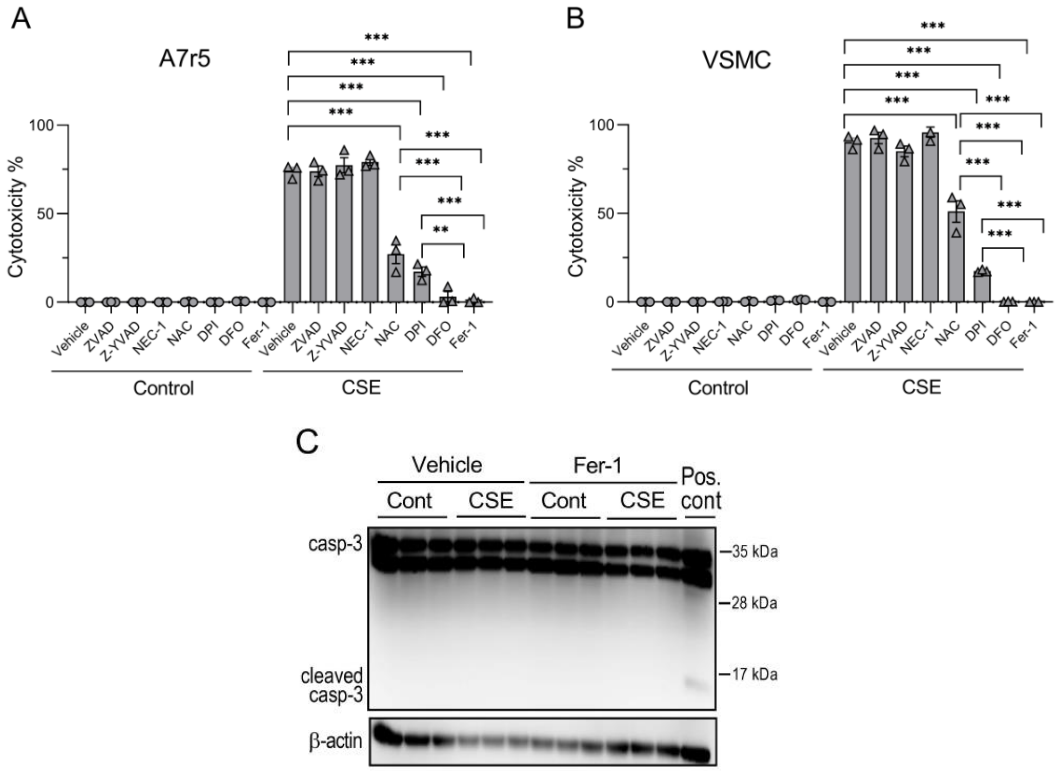

Figure 6. CSE-induced ferroptosis

A7r5 cells (A) and primary VSMCs (B) were treated with CSE (0.8 mg/mL) for 4 h in the presence or absence of Z-VAD (20 μM), Z-YVAD (20 μM), Nec-1 (10 μM), NAC (200 μM), DPI (10 μM), DFO (100 μM), and Fer-1 (5 μM). Cytotoxicity was assessed by an LDH release assay (n = 3). (C) A7r5 cells were treated with CSE for 2 h in the presence or absence of Fer-1. Cell lysates were analyzed by Western blot analysis for cleaved caspase-3 (n = 3). Cells treated with staurosporine (0.5 μM) for 20 h were used as a positive control (Pos. cont). Data are expressed as the mean ± SEM. $^{**}p < 0.01$, $^{***}p < 0.001$.

Since CSE induces inflammatory responses [46], we performed real-time RT-PCR analysis and showed that CSE significantly elevated mRNA levels of IL-1β, IL-6, and TNF-α, in A7r5 cells (Fig. 7A). To rule out the possibility of contamination of CSE with bacterial molecules, we used polymyxin-B, an antibiotic that sequesters and thereby inactivates contaminating lipopolysaccharide (LPS), and confirmed that treatment with polymyxin-B had no effect on CSE-induced upregulation of these

inflammatory cytokines in A7r5 cells (Fig. 7B).

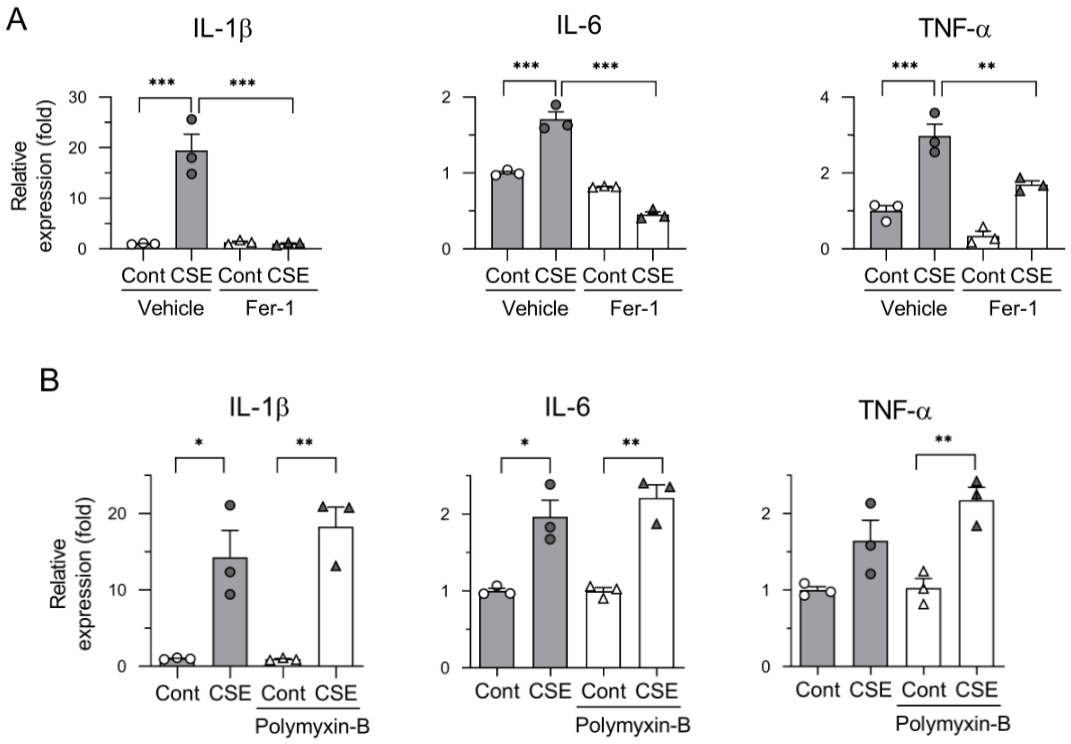

Figure 7. CSE-induced inflammatory responses

(A) A7r5 cells were treated with CSE (0.8 mg/mL) for 4 h. The mRNA levels of IL-1β, IL-6, TNF-α were assessed by real-time RT-PCR analysis. (B) A7r5 cells were treated with CSE (0.8mg/mL) for 4 h in the presence of polymyxin-B (100 U/mL). The mRNA levels of IL-1β, IL-6, TNF-α were assessed by real-time RT-PCR analysis. Data are expressed as the mean ± SEM. *$p < 0.05$, **$p < 0.01$, ***$p < 0.001$.

Furthermore, CSE increased the mRNA levels of MMP-2, MMP-9, and TIMP-1, which are involved in the degradation of extracellular matrix components (Fig. 8A). Fer-1 significantly inhibited the CSE-induced upregulation of these cytokines and MMPs. These results suggest that CSE induces inflammatory responses and matrix degradation at the vascular wall.

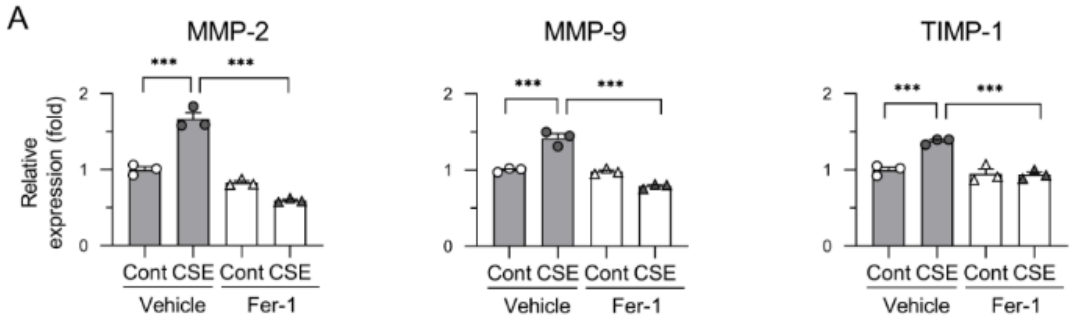

Fig.8 CSE-induced MMP-2, MMP-9, and TIMP1 expression

(A) A7r5 cells were treated with CSE (0.8 mg/mL) for 4 h. The mRNA levels of MMP-2, MMP-9, and TIMP-1 were assessed by real-time RT-PCR analysis. Data are expressed as the mean ± SEM. ***$p < 0.001$.

3-3. Mechanisms of CSE-induced ferroptosis

Given that ferroptosis is essential for CSE-induced VSMC death, we assessed key features of ferroptosis, including lipid peroxidation and the upregulation of Ptgs2 mRNA (encoding COX-2) [41]. CSE treatment markedly increased lipid peroxidation determined by C11 BODIPY$^{581/591}$ dye in A7r5 cells and primary VSMCs, and this increased lipid peroxidation was almost completely inhibited by Fer-1 (Fig. 9A, B and C). Real-time RT-PCR analysis showed that CSE upregulated Ptgs2 expression in A7r5 cells, and this Ptgs2 upregulation was inhibited by Fer-1 (Fig. 9D).

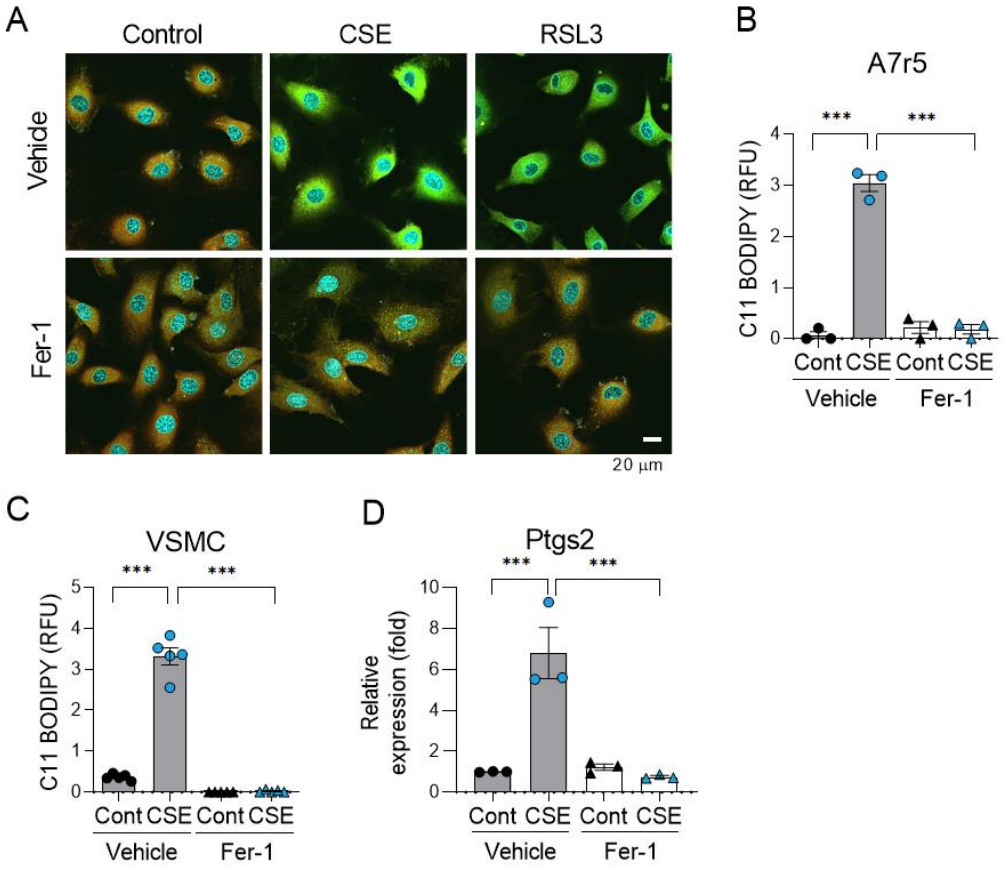

Figure 9. Mechanisms of CSE-induced ferroptosis

(A, B, and C) A7r5 cells and primary rat VSMCs (D) were treated with CSE (0.8 mg/mL) for 1 h in the presence or absence of Fer-1 (5 μM). Lipid peroxidation was assessed by C11 BODIPY$^{581/591}$ staining. (A) Representative images of C11 BODIPY$^{581/591}$ staining. (B and C) Quantitative analysis of BODIPY$^{581/591}$ fluorescence intensity in A7r5 and primary VSMCs. (D) Ptgs2 mRNA levels in A7r5 cells treated with CSE for 4 h.

Since ferroptosis occurs when GPX4 is inhibited either directly through its expression level or indirectly through the unavailability of GSH [38], we performed western blotting for GPX4 and showed that CSE and/or Fer-1 did not affect the GPX4 levels in A7r5 cells (Fig. 10A). To further investigate the role of GPX4, we established GPX4-overexpressing A7r5 cells using a lentiviral system (Fig. 10B); however, CSE-induced ferroptosis was not substantially influenced by GPX4 overexpression (Fig. 10C and D).

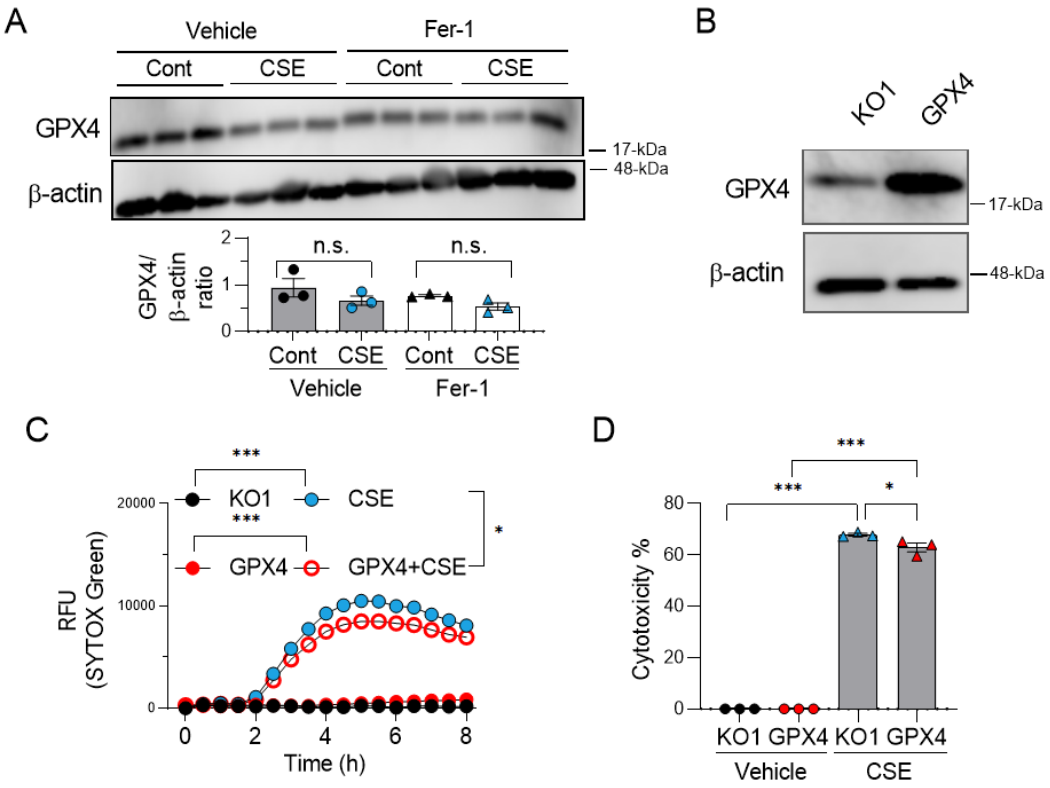

Fig. 10 GPX4 did not involve in CSE-induced ferroptosis

(A) GPX4 protein levels in A7r5 cells treated with CSE for 2 h in the presence or absence of Fer-1. The GPX4 protein levels were quantified (n = 3). (B) Overexpression of GPX4 in A7r5 cells. (C and D) GPX4- and KO1-overexpressing A7r5 cells were treated with CSE for 4 h. Cell death and cytotoxicity were assessed with SYTOX Green and by an LDH release assay, respectively (n = 3). Data are expressed as the mean ± SEM. *$p < 0.05$, **$p < 0.01$, ***$p < 0.001$.

Previous studies have shown that intracellular GSH depletion is accompanied by cytotoxicity of cigarette smoke [47-48], and it also causes ferroptotic cell death in certain cell types [49]. Therefore, we assessed intracellular GSH levels and found that these levels were decreased entirely in CSE-treated A7r5 cells, which was not restored by Fer-1 (Fig. 11B). Besides, CSE-induced GSH depletion preceded the morphological changes associated with cell death (Fig. 11A and B).

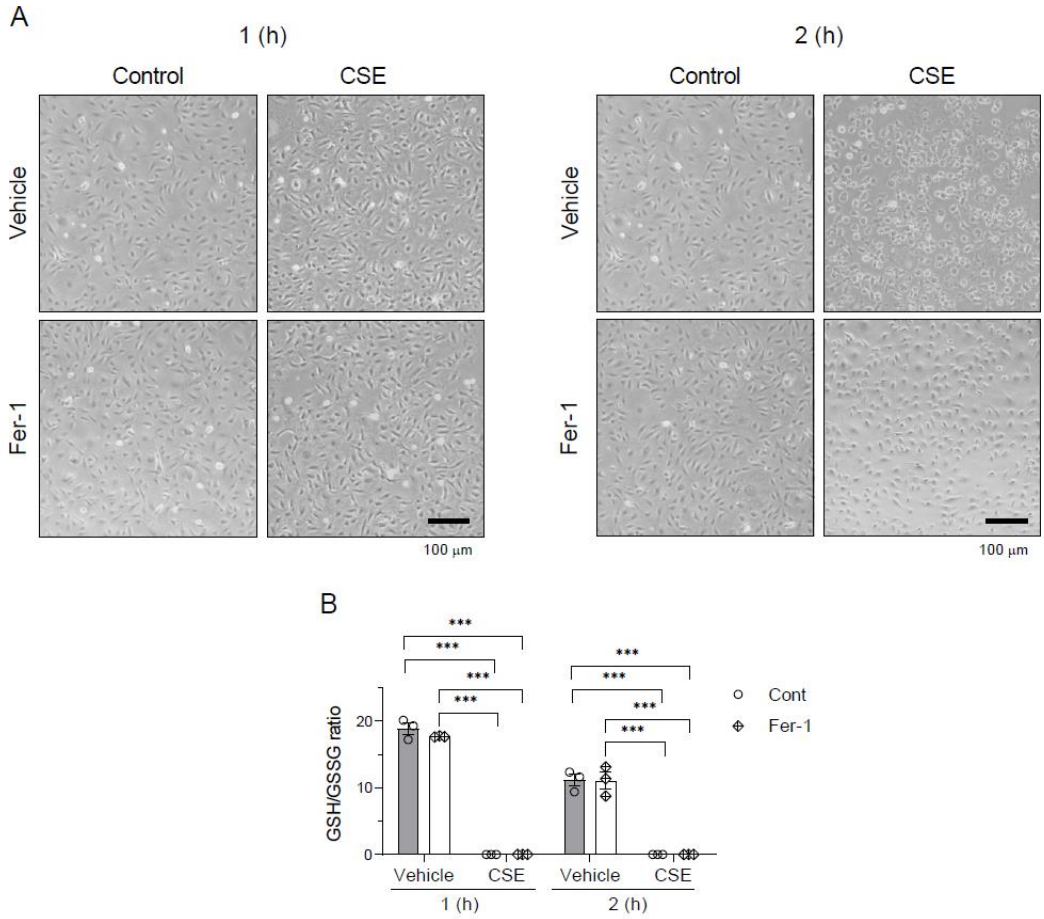

Fig.11 Effects of CSE on morphological changes and intracellular GSH levels
Light microscopic image of A7r5 cells at 1 and 2 h after CSE treatment. (B) GSH/ GSSG ratio in A7r5 cells at 1 and 2 h after CSE treatment (n = 3). Data are expressed as the mean ± SEM. ***$p <$ 0.001.

3-4. ACR and MVK as responsible factors for CSE-induced ferroptosis

CSE contains numerous chemical constituents that have cytotoxic properties in various cell types. Among them, ACR, MVK, and CPO have been shown to be major cytotoxic factors in CSE [50]. Therefore, we examined whether ACR, MVK, and CPO could induce ferroptosis in A7r5 cells, and found that ACR and MVK induced cell death in a time- and dose-dependent manner (100–300 μM) using an SYTOX Green assay; ACR- and MVK-induced cell death was inhibited entirely by Fer-1 (Fig. 12A and B). Similar changes were observed regarding cytotoxicity determined by an LDH release assay. In contrast, CPO failed to induce cell death in A7r5 cells (Fig. 12C). These

findings indicate that ACR and MVK are responsible factors for CSE-induced VSMC ferroptosis.

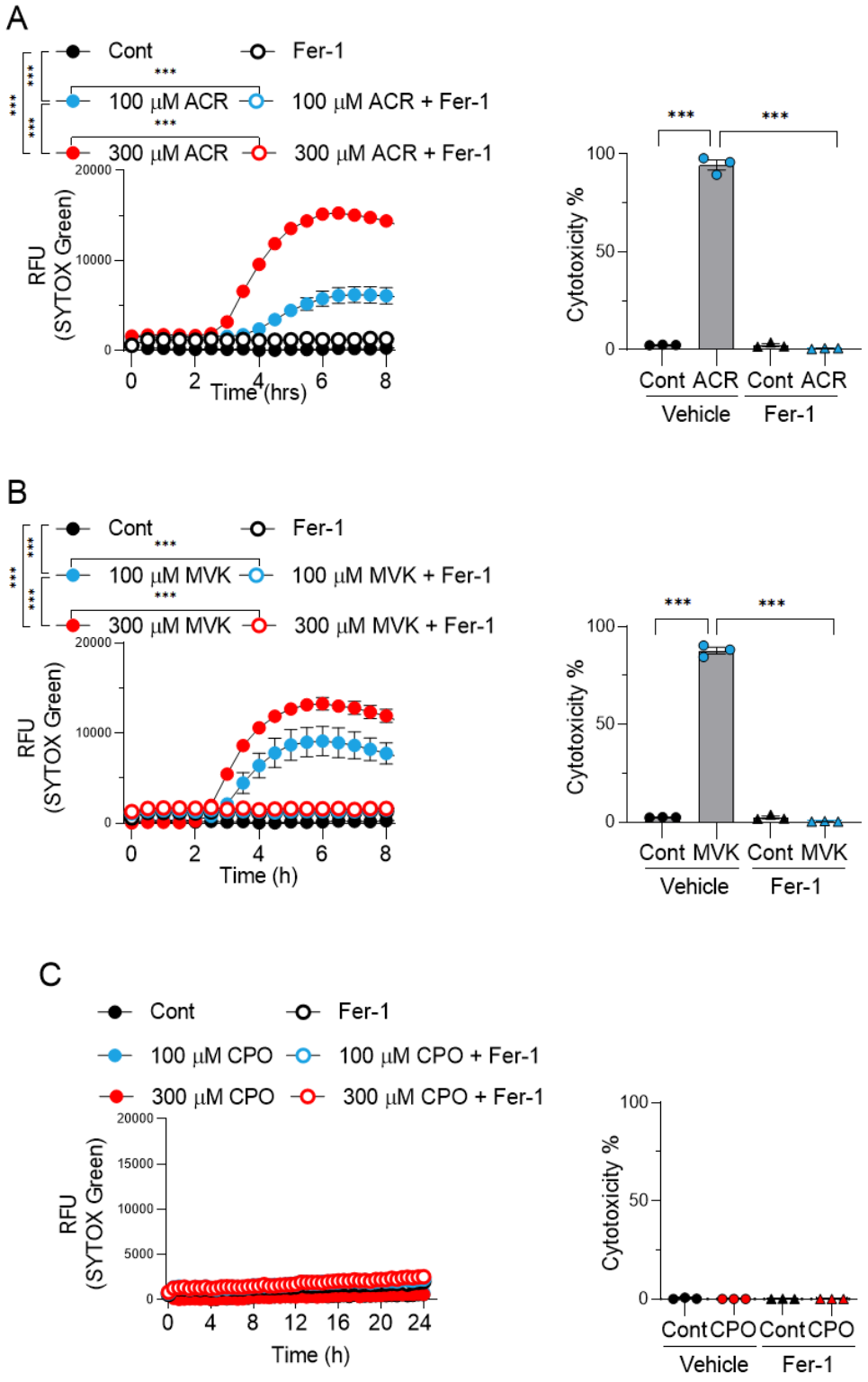

Figure 12. ACR and MVK as responsible factors for CSE-induced ferroptosis

A7r5 cells were treated with ACR (A, 100 and 300 μM), MVK (B, 100 and 300 μM), or CPO (C, 100 and 300 μM) for 6 h in the presence or absence of Fer-1 (5 μM). Cell death and cytotoxicity

were assessed with SYTOX Green and by an LDH release assay, respectively (n = 3). Data are expressed as the mean ± SEM. ***$p < 0.001$.

3-5. Effect of CSE on medial VSMC loss in ex vivo aortas

Epidemiological studies have indicated that cigarette smoking is a major risk factor for the development of AA and AD [51-53]. To investigate the potential role of CSE-induced VSMC ferroptosis in AA and AD development, we treated *ex vivo* cultured aortic rings with CSE in the presence or absence of Fer-1 and assessed cell death by SYTOX Orange staining. SYTOX Orange-positive cells were significantly increased at the aortic wall of CSE-treated aortas, compared to those in control aortas (Fig. 13A and B). In accordance with this result, LDH release was significantly increased in the culture media of CSE-treated aorta (Fig. 13C). Furthermore, the increased cell death determined by SYTOX Orange and LDH release was partially but significantly restored by Fer-1 treatment (Fig. 13 A–C).

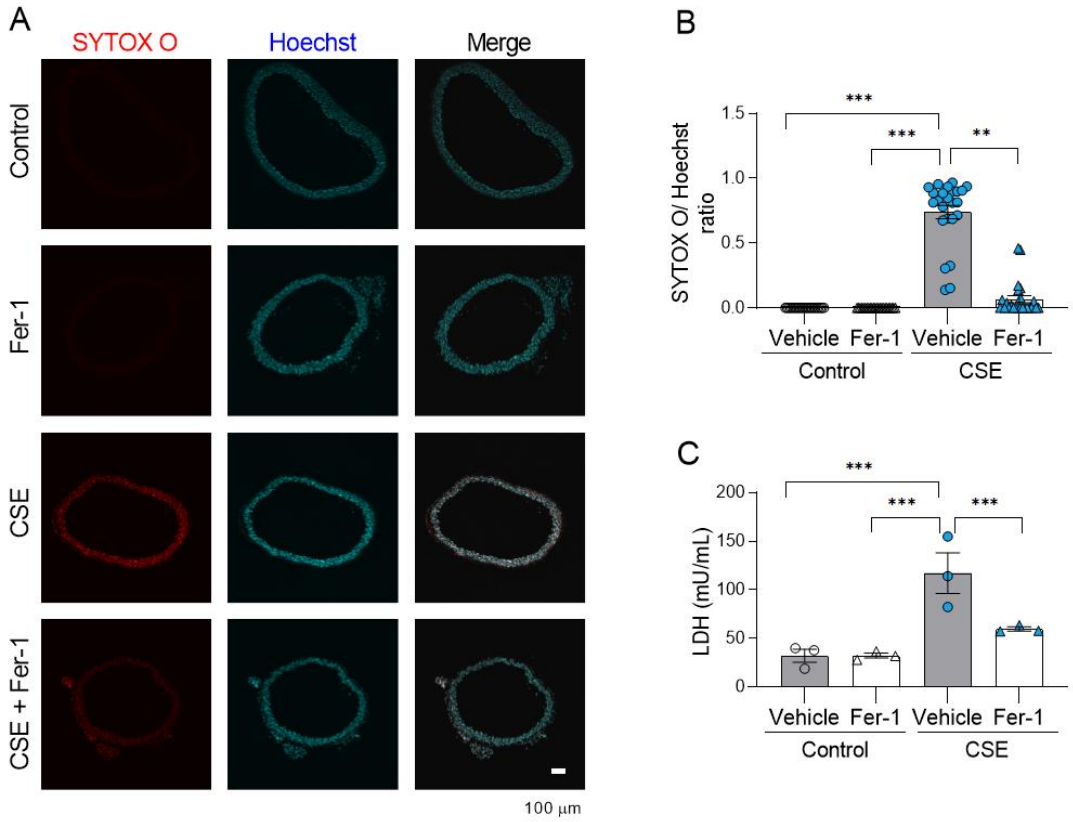

Figure 13. Effect of CSE on medial VSMC loss in ex vivo aortas

Ex vivo aortic rings were treated with CSE in the presence or absence of Fer-1 (5 μM) for 8 h. (A) Representative images of SYTOX Orange staining. (B) Quantitative analysis of SYTOX Orange-positive cells/nuclei was performed. (C) LDH release in the culture media was assessed.

The expression of 4-HNE, a secondary product of lipid peroxidation, was visualized in the CSE-treated aortas (Fig. 14).

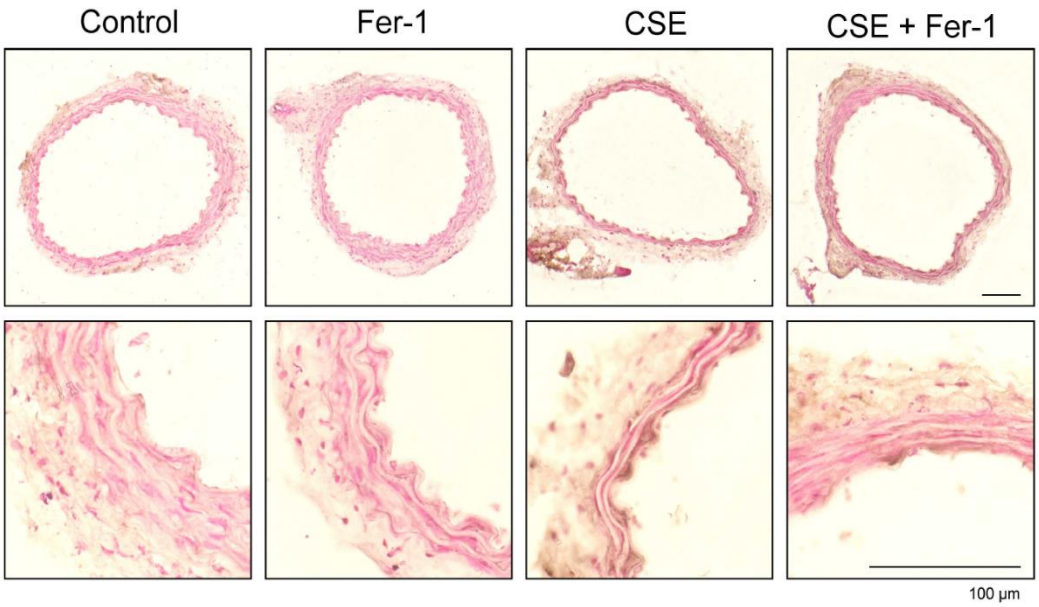

Fig 14. Effect of CSE on lipid peroxidation in ex vivo aorta

Ex vivo aortic samples were treated with CSE (0.8mg/mL) for 3 h. Fer-1 (10 μm/mL) treatment were applied for 3 h prior to CSE treatment. A light microscopic image of 4-HNE immunostaining was shown.

Interestingly, EVG staining showed that the amount of medial VSMCs was substantially reduced in CSE-treated aortas, and this medial VSMC loss was also partially restored by Fer-1 treatment (Fig. 15A).

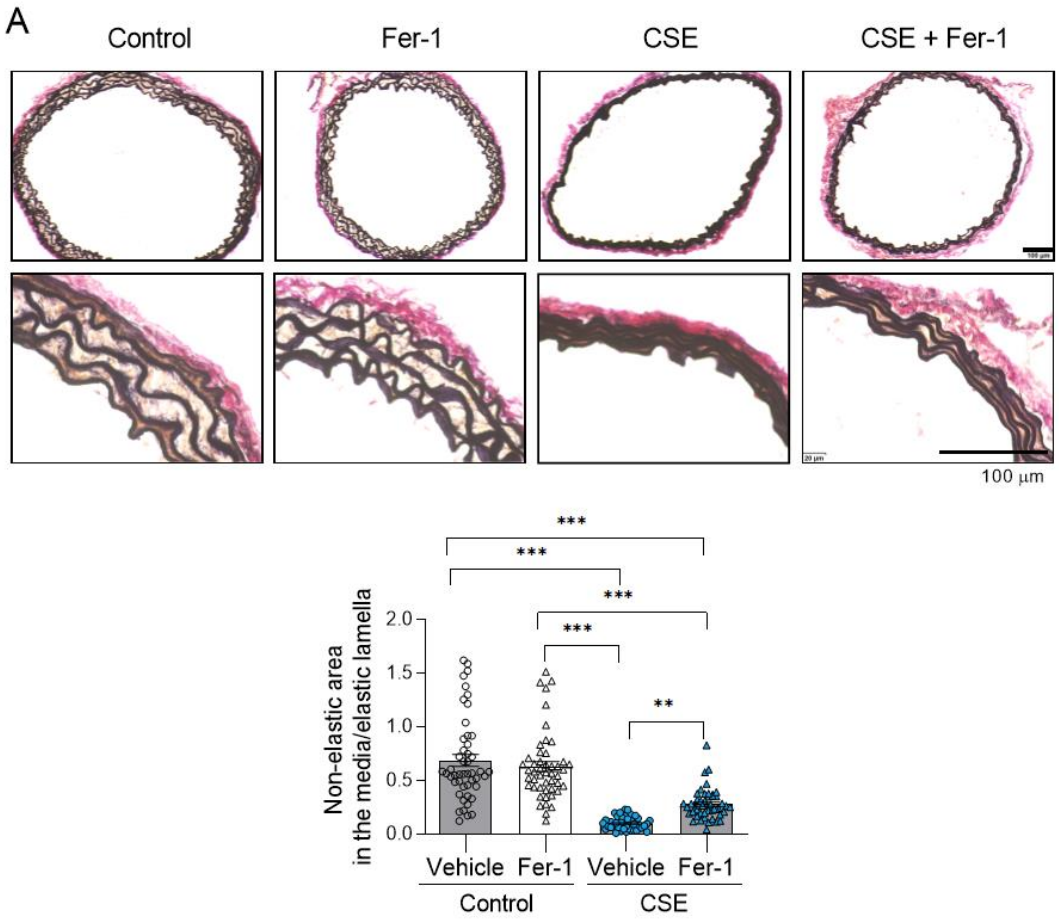

Figure 15. Effect of CSE on medial loss in ex vivo aortas

Ex vivo aortic rings were treated with CSE in the presence or absence of Fer-1 (5 μM) for 16 h. (A) Representative images of EVG staining and quantitative analysis of medial cell loss (non-elastic area/elastic lamella in the media) was performed. Data are expressed as the mean ± SEM. $^{**}p < 0.01$, $^{***}p < 0.001$.

To further analyze morphological changes in medial VSMCs, we performed TEM analysis of *ex vivo* aortas, and observed that VSMCs among the elastic lamina were severely damaged in CSE-treated aortas, while elastic laminae in tunica media were preserved (Fig. 16, left column). The nuclear membranes appeared to be intact, but nuclear chromatin condensation was detected in VSMCs of the CSE-treated aortas (Fig. 16, second column from the left). In addition, the loss of mitochondria and myofilaments were prominent, and a small number of residual mitochondria were fragmented in CSE-treated VSMCs (Fig. 16, right column). In contrast, some VSMCs

pretreated with Fer-1 prior to CSE showed retained cytoplasmic structures such as myofilaments and mitochondria, suggesting that Fer-1 helped to protect against severe CSE-induced VSMC damage.

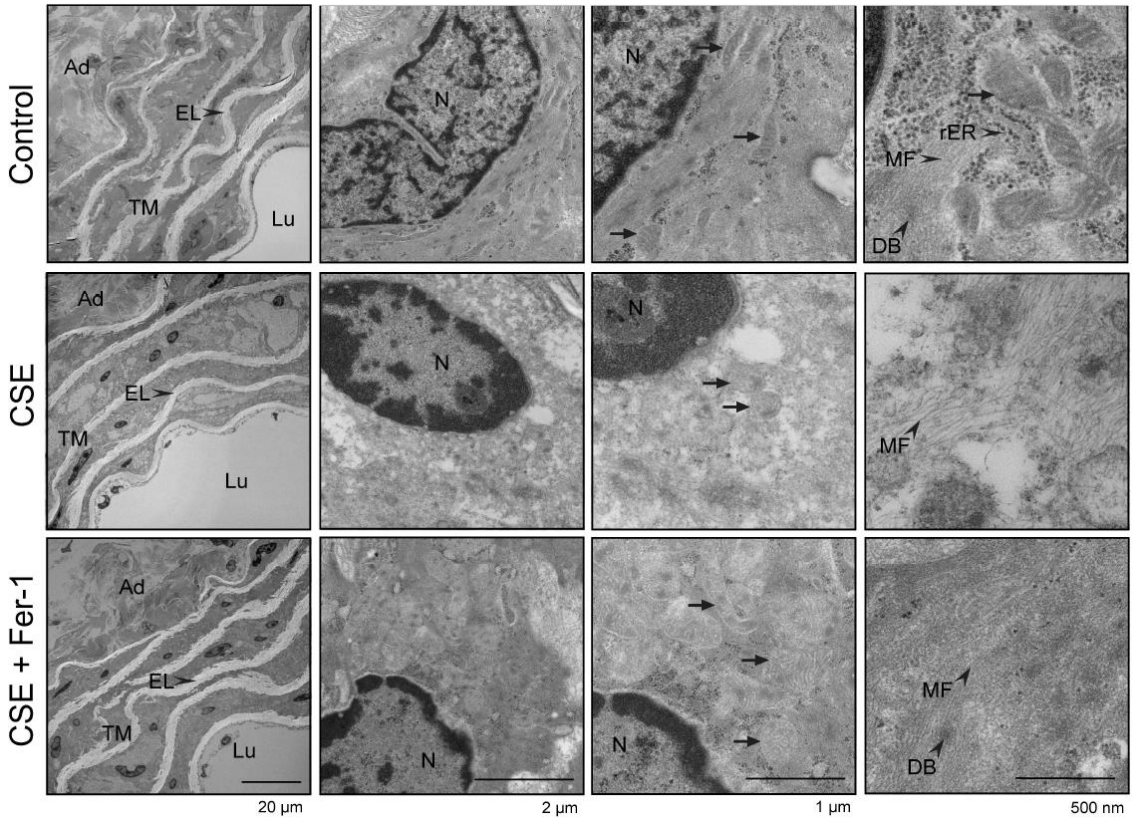

Figure 16. TEM analysis of ex vivo aortas treated with CSE

Ex vivo aortic rings were treated with CSE in the presence or absence of Fer-1 (5 μM) for 6 h. Representative images of TEM analysis are shown. Arrows indicate mitochondria. Ad, adventitia; TM, tunica media, Lu, lumen, N, nucleus; MF, myofilament; DB, dense body, rER, rough endoplasmic reticulum.

4. Discussion

The major findings of this study are as follows: 1) CSE induced cell death in VSMCs in a dose- and time-dependent manner, which was entirely abolished by ferroptosis-specific inhibitors or iron chelator, but not by inhibitors of apoptosis, pyroptosis, or necroptosis; 2) CSE-induced VSMC death was also partially abolished by the GSH precursor NAC; 3) CSE increased lipid peroxidation and Ptgs2 mRNA expression, which are key features of ferroptosis; 4) CSE markedly decreased

intracellular GSH levels; 5) ACR and MVK, major cytotoxic factors in CSE, induced VSMC ferroptosis; and 6) CSE induced severe damage and loss of medial VSMCs in *ex vivo* cultured aortas. These findings identified that ferroptosis is the mechanism responsible for CSE-induced cytotoxicity in VSMCs, and demonstrated that CSE-induced ferroptosis contributes to the development of AA and AD. Since cigarette smoke is a major risk factor for these aortic disorders, our study also suggests that ferroptosis is a novel therapeutic target for preventing cigarette smoke-related aortic disorders.

Cigarette smoking has a substantial impact on the development of AA and AD. However, the mechanism by which smoking induces AA and AD is not yet fully understood. The loss of medial VSMCs at the arterial wall is one of the key pathophysiologic features in AA and AD, and presumably leads to arterial wall weakening and subsequent dilatation and dissection [54]. In this regard, while CSE has been shown to induce cytotoxicity in various types of cells [31], the precise mechanism of CSE-induced cytotoxicity is not yet fully understood. In the present study, we identified ferroptosis as the mechanism that is responsible for CSE-induced VSMC cytotoxicity. Previous studies suggested that apoptosis is involved in this process; however, the presence of apoptosis in CSE-induced cell death has been questioned [35]. Indeed, we observed that CSE-induced cell death was not inhibited by inhibitors of apoptosis (Z-VAD) or other forms of cell death, such as pyroptosis (Z-YVAD) and necroptosis (Nec-1).

On the other hand, CSE-induced cell death was significantly inhibited by an iron chelator (DFO), GSH precursor (NAC), and NADPH oxidase inhibitor (DPI), which is in accordance with the notion that iron-dependent lipid peroxidation plays a critical role in the initiation of ferroptosis [37]. The TEM findings showing prominent alterations in mitochondrial morphology also support the idea that ferroptosis is involved in CSE-

induced cell death. Consistent with our findings, Park *et al*. [55] recently reported that whole cigarette smoke condensates might induce ferroptosis in bronchial epithelial cells by a KEGG pathway analysis. Yoshida *et al*. [42] also recently reported that CSE induces ferroptosis in lung epithelial cells, contributing to chronic obstructive pulmonary diseases' pathogenesis. Collectively, ferroptosis plays a pivotal role in cigarette smoking-related cytotoxicity in VSMCs and lung epithelial cells.

In addition to VSMC death, inflammation has been shown to play an essential role in AA's pathogenesis [56]. We determined that the expression of inflammatory cytokines is elevated in VSMCs soon after CSE treatment, suggesting that CSE stimulates chemokine release, which recruits inflammatory cells, such as monocytes/macrophages neutrophils, to the aortic wall and further enhances inflammatory responses. CSE-induced ferroptosis also triggers the extracellular release of cellular contents, such as nucleic acid and high mobility group box 1 (HMGB1), known as danger signals [57]. The released danger signals are then recognized by innate immune receptors, including Toll-like receptors on recruited macrophages, and eventually, potentiate inflammation.

Degradation of ECM by MMPs are well-established changes and contribute to the pathogenesis of AA. Histologically, elastolysis is one of the earliest observable events in aneurysmal tissue. MMP-2 and -9 are appeared to play an important role in elastic lamellae fragmentation [58]. Previous studies indicated that MMP-2 is the dominant gelatinase in small-sized aneurysms, and MMP-9 becomes important in the later stages of aneurysm formation. We had found that both MMP-2 and -9 mRNA expression levels were significantly elevated after CSE treatment in VSMCs. Furthermore, this elevation was inhibited by Fer-1 treatment.

It is crucial to consider the activity of MMPs in relation to their inhibitor TIMPs during aneurysm progression. In previous studies, significant amounts of TIMP-1 and -

2 mRNA expression have been detected in human AAs [59]. In addition, increased expression levels of TIMP-1 are shown to be highly correlated to medium-large human AAs. In our experimental setting significant increase of TIMP-1 mRNA expression after CSE treatment had been observed. This results regarding the increase of MMP-2, -9, and TIMP-1 mRNA expression in VSMCs treated with CSE might indicate the importance of cigarette smoking on proteolytic state of AA.

Interestingly, CSE-induced upregulation of these cytokines and MMPs was inhibited by Fer-1. Although Fer-1 was previously thought to be a lipoxygenase (LOX) inhibitor, it is now considered to be a radical trapping agent in membrane phospholipid [60]. In this regard, lipid peroxidation has been shown to regulate redox-sensitive transcription factors such as nuclear factor kappa-light-chain-enhancer of activated B cells (NF-κB) and activator protein-1 (AP-1), which play a crucial role in inflammatory cytokine expression [61]. Taken together, CSE-induced inflammation and matrix degradation contribute to the development of AA and AD.

GPX4 converts lipid hydroperoxides to nontoxic lipid alcohol, which utilizes GSH as a cosubstrate. Pharmacological inhibition or genetic deletion of GPX4 promotes ferroptosis. RSL-3 is a small molecule that is a well-known ferroptosis inducer through its direct inhibitory effect on GPX4, resulting in lipid ROS accumulation. Moreover, system Xc inhibitor Erastin could induce ferroptosis through inhibiting GSH synthesis. We did not find a change in GPX4 protein level after CSE treatments. Moreover, GPX4 overexpression in VSMCs did not rescue CSE-induced ferroptosis. Indeed, CSE treatment had exhausted the intracellular GSH level even before the cellular morphologic changes occur, suggesting that GSH depletion is the primary mechanism involved in the induction of VSMC ferroptosis. Moreover, this result is consistent with the study describing cigarette smoke-induced depletion of GSH, reducing the defenses against the oxidant-induced cellular injury, and causes an increase of cell death [62].

Furthermore, previous studies have suggested that ACR and MVK, primary cytotoxic compounds in CSE, can form conjugates with GSH rapidly [63-64]. In line with previous findings, we observed depletion of GSH in response to CSE exposure within one hour. Furthermore, NAC treatment rescued cells from death, further supporting the notion that GSH levels are a critical determinant for ferroptosis.

Our *ex vivo* experiment results showed that CSE caused medial VSMC loss, which was determined by EVG, and further confirmed by electron microscopy analysis. TEM results revealed severe mitochondrial damage and myofibril loss in medial VSMCs of CSE-treated aortas. All of these manifestations were partially restored by Fer-1. These findings demonstrate that ferroptosis is responsible for CSE-induced VSMC death and suggest that ferroptosis is a potential therapeutic target for preventing AA and AD.

The cigarettes used to generate CSE contains 17 mg tar per cigarette [31], indicating that the dosage of CSE (0.8 mg/mL) used in this study is approximately 235 times higher than that of one cigarette if the smoke was absorbed and distributed in 5000 mL blood. In general, chronic smokers are known to smoke more than 20 cigarettes per day, and thus the CSE dosage is just ten times higher than that in the blood of chronic smokers. In this regard, lipid peroxidants, a hallmark of ferroptosis, are increased in the plasma, urine, and arterial tissue of chronic smokers. Moreover, ACR and MVK have been reported to be stable and cumulative [34]. Therefore, we assume that CSE-induced ferroptosis can occur in the aortic walls of chronic smokers and contribute to AA and AD development.

We observed an increase in ferroptotic VSMCs and the corresponding decrease in medial thickness in CSE treated ex-vivo aortas in contrast to control aortas. Previous studies were demonstrated that VSMC apoptosis is the plausible mechanism of medial

layer degeneration [65-66]. However, in this study, we had found that VSMC ferroptosis might occur in chronic smokers' aortic walls.

Lipid peroxidation is one of the hallmark events that occur during ferroptosis. In association with this, our results also showed high levels of lipid peroxidation in both in VSMCs and in ex vivo aorta treated with CSE, which were significantly inhibited by Fer-1. According to previous studies, these results showed that lipid peroxidation occurred in greater extents in smokers than non-smokers [67-68]. This phenomenon might also further confirm ferroptosis involvement in aortic medial VSMC loss due to cigarette smoking.

Several limitations of this study should be noted. First, we clearly showed that CSE induced VSMC ferroptosis *in vitro* and caused medial VSMC loss in *ex vivo* aortas; however, the *in vivo* effect of CSE on the development of aortic aneurysm remains to be examined. Although no previous report has described animal models of AA and AD induced by CSE treatment, chronic CSE treatment for 2–5 months has been shown to accelerate atherogenesis in atherosclerosis-prone mice and rabbits [69-70]. Interestingly, the atherosclerotic lesions in CSE-treated rabbits were significantly decreased by treatment with vitamin E [70], a potent inhibitor of ferroptosis [71]. Moreover, Sawada *et al*. [72] reported that iron is involved in abdominal AA formation's pathophysiology with oxidative stress and inflammation. Thus, it is likely that ferroptosis is involved in the development of smoking-related atherosclerosis and AA. Second, although we showed that intracellular GSH depletion after CSE exposure leads to lipid peroxidation, the subcellular locations, such as plasma membrane, mitochondria, and endoplasmic reticulum, where lipid peroxidation occurs during ferroptosis have not been identified [73]. GSH is freely distributed in the cytosol and can be compartmentalized in mitochondria and endoplasmic reticulum [74]. On the other hand, a reduced form of GSH is predominantly detected in cytoplasm and mitochondria [75], suggesting that

CSE-induced lipid peroxidation occurs in mitochondria and/or plasma membrane. In this regard, Gao *et al*. [76] reported that mitochondria play a crucial role in ferroptosis induced by cysteine deprivation, a precursor of GSH synthesis. Because we observed plasma membrane rupture shown by SYTOX staining and significant damage of mitochondria, we postulate that CSE-induced lipid peroxidation and subsequent ferroptosis occur in the mitochondria. Further investigations are necessary to elucidate the precise mechanism underlying CSE-induced ferroptosis and its role in the pathophysiology of AA and AD.

5. Conclusion

In conclusion, we demonstrated that ferroptosis plays an essential role in CSE-induced VSMC cytotoxicity through intracellular GSH depletion *in vitro* and CSE induced medial VSMC damage and loss in *ex vivo* aortas. These findings provide new insights into the mechanism of cigarette smoking-related cytotoxicity and suggest that ferroptosis is a potential therapeutic target for preventing AA and AD.

6. References

1. Prisant LM, Mondy JS, Abdominal Aortic Aneurysm. *The Journal of Clinical Hypertension*, 6(2):85-89, 2004
2. Gillum RF, Epidemiology of aortic aneurysm in the United States. *Journal of Clinical Epidemiology*, 48(11):1289-1298, 1995
3. El-Hamamsy, Magdi HY, Cellular and molecular mechanisms of thoracic aortic aneurysms. *Nature Reviews Cardiology*, 6(12):771-786, 2009
4. Glagov S, Wolinsky H, A lamellat unit of aortic medial structure and function in mammals. Circulation Research, 20:99-111, 1967

5. Shimizu K, Mitchell RN, and Libby P, Inflammation and cellular immune responses in abdominal aortic aneurysms. *Arteriosclerosis Thrombosis and Vascular Biology*, 26(5):987-994, 2006
6. Menashi S, Campa JS, Greenhalgh RM, Powell JT, Collagen in abdominal aortic aneurysm: typing, content, and degradation. *Journal of Vascular Surgery*, 6(6):578-582, 1987
7. Lopez-Candales A, Holmes DR, Liao S, Scott MJ, Wickline SA, Thompson RW, Decreased vascular smooth muscle cell density in medial degeneration of human abdominal aortic aneurysms. *American Journal of Pathology*,150(3):993-1007, 1997
8. Edward C, Matthew MT, Joseph DW, Richard WW, Saiqa S, Ian ML, Gillian WC, Abdominal aortic aneurysm rupture is associated with increased medial neovascularization and overexpression of proangiogenic cytokines. *Arteriosclerosis, Thrombosis and Vascular Biology*, 26(9):2077-20820, 2006
9. Campa JS, Greenhalgh RM, Powell JT, Elastin degradation in abdominal aortic aneurysms. *Atherosclerosis*, 65(1–2):13-21, 1987
10. Narayanan AS, Sandberg LB, Ross R, Layman DL, Elastin Synthesis in Arterial Smooth Muscle Cell Culture. *The Journal of Cell Biology*, 68(9):411-419, 1976
11. Vardulaki KA, Walker NM, Day NE, Duffy SW, Ashton HA, Scott RA, Quantifying the risks of hypertension, age, sex and smoking in patients with abdominal aortic aneurysm. *British Journal of Surgery*, 87(2):195-200, 2000
12. Brown LC, Powell JT, Risk Factors for Aneurysm Rupture in Patients Kept Under Ultrasound Surveillance. *Annals of Surgery*, 230(3):289, 1999

13. Castleden WM, Mercer JC, Abdominal aortic aneurysms in Western Australia: Descriptive epidemiology and patterns of rupture. *British Journal of Surgery*, 72(2):109-112, 1985
14. Reed WW, Hallett Jr JW, Damiano MA, Ballard DJ, Learning From the Last Ultrasound: A Population Based Study of Patients With Abdominal Aortic Aneurysm. *Archives of Internal Medicine*,157(18):2064-2068, 1997
15. McFarlane MJ, The Epidemiologic Necropsy for Abdominal Aortic Aneurysm. *The Journal of the American Medical Association*, 256(16):2085-2088, 1991
16. Lederle FA, Jonhson GR, Wilson SE, Chute EP, Littooy FN, Bandyk D, Krupski WC, Barone GW, Acher CW, Ballard DJ, Prevalence and Associations of Abdominal Aortic Aneurysm Detected through Screening. *Annals of Internal Medicine*,126(6):441-449, 1997
17. Amélie P, Gregory TJ, Dianna MM, Genetics of Thoracic and Abdominal Aortic Diseases. *Circulation Research*, 124 (4):588-606, 2019
18. David GA, Vishwanath B, Matthew B. Mechanism of vascular disease: A Reference Book for Vascular Specialists. *Cambridge university press*: 226-234, 2007
19. Prediman KS, Inflammation, Metalloproteinases, and Increased Proteolysis: An emerging Pathophysiological Paradigm in Aortic Aneurysm. *Circulation Research*, 96(7):2115-2117, 1997
20. Herron GS, Unemori E, Wong E, Rapp JH, Hibbs MH, Stoney RJ. Connective tissue proteinases and inhibitors in abdominal aortic aneurysms. Involvement of the vasa vasorum in the pathogenesis of aortic aneurysms. *Arterosclerosis, Thrombosis, and Vascular Biology*,11(6):1667-1677, 1991
21. Holmes DR, Liao S, Parks WC, Thompson RW, Medial neovascularization in abdominal aortic aneurysms: A histophatologic marker of aneurysmal

degeneration with pathophysiologic implications. *Journal of Vascular Surgery*, 21(5):761-772, 1995

22. Ploingarm P, Malgorzata F, Rachael F, Marc D, Geert WS, Ehsan N, Chris R, Michael J, Barend M, Leon S. Role of Vascular Smooth Muscle Cell Phenotypic Switching and Calcification in Aortic Aneurysm Formation Involvement of Vitamin K-Dependent Processes. *Arteriosclerosis, Thrombosis, and Vascular Biology*, 39:1351-1368. 2019
23. Keeling WB, Armstrong PA, Stone PA, Bandyk DF, Shames ML, An overview of matrix metalloproteinases in the pathogenesis and treatment of abdominal aortic aneurysms. *Vascular and Endovascular Surgery*, 39:457-464, 2005
24. McMIllan WD, Pearce WH, Incraesed plasma levels of metalloproteinase-9 are associated with abdominal aortic aneurysms. *Journal of Vascular Surgery*, 29:122-127, 1999
25. Nakamura M, Tachieda R, Niinuma H, Ohira A, Endoh S, Hiramori K, Makita S, Circulating biochemical marker levels of collagen metabolism are abnormal in patients with abdominal aortic aneurysm. *Angiology*, 51:385-92, 2000
26. Yamanouchi D, Morgan S, Kato K, Lengfeld J, Zhang F, Liu B. *Arteriosclerosis, Thrombosis, and Vascular Biology*, 30:702–707, 2010
27. Wang Q, Zhou T, Liu Z, Ren J, Phan N, Gupta K, Danielle MS, Morgan S, Assa C, Kent KC & Liu B. Inhibition of Receptor-Interacting Protein Kinase 1 with Necrostatin–1s ameliorates disease progression in elastase-induced mouse abdominal aortic aneurysm model. *Scientific Reports*,7:42159, 2017
28. Nordon IM, Hinchliffe RJ, Loftus IM & Thompson MM. Pathophysiology and epidemiology of abdominal aortic aneurysms *Nature Reviews Cardiology*, 8:92–102, 2011

29. Norman PE and Curci JA, Understanding the effects of tobacco smoke on the pathogenesis of aortic aneurysm, *Arteriosclerosis, Thrombosis, and Vascular Biology.* 33(7):1473–1477, 2013

30. Rafacho BP, Azevedo PS, Polegato BF. Tobacco smoke induces ventricular remodeling associated with an increase in NADPH oxidase activity. *Cellular Physiology and Biochemistry*, 27(3-4):305-312, 2011

31. Higashi T, Mai Y, Noya Y, Horinouchi T, Terada K, Hoshi A, Nepal P, Harada T, Horiguchi M, Hatate C, Kuge Y, Miwa SA. Simple and rapid method for standard preparation of gas phase extract of cigarette smoke. *PLoS One,* 9:e107856, 2014

32. Liu C, McAdam KG, Perfetti TA. Some recent topics in cigarette smoke science. *Mini-Reviews in Organic Chemistry,* 8:349-359, 2011

33. Yamaguchi Y, Nasu F, Harada A, Kunitomo M. Oxidants in the gas phase of cigarette smoke pass through the lung alveolar wall and raise systemic oxidative stress. *Journal Pharmacological Sciences,* 103:275-282, 2007

34. Noya Y, Seki K, Asano H, Mai Y, Horinouchi T, Higashi T, Terada K, Hatate C, Hoshi A, Nepal P, Horiguchi M, Kuge Y, Miwa S. Identification of stable cytotoxic factors in the gas phase extract of cigarette smoke and pharmacological characterization of their cytotoxicity. *Toxicology,* 314:1-10, 2013

35. Bernhard D, Pfister G, Huck CW, Kind M, Salvenmoser W, Bonn GK, Wick G. Disruption of vascular endothelial homeostasis by tobacco smoke: impact on atherosclerosis. *FASEB J,* 17:2302-2304, 2003

36. Franco R and Cidlowski JA. Glutathione Efflux and Cell Death. Antioxidants & Redox Signalling, 17(12):1694-1713, 2012

37. Dixon SJ, Lemberg KM, Lamprecht MR, Skouta R, Zaitsev EM, Gleason CE, Patel DN, Bauer AJ, Cantley AM, Yang WS, Morrison B, Stockwell BR. Ferroptosis: an iron-dependent form of nonapoptotic cell death. *Cell,* 149:1060-1072, 2012

38. Kagan VE, Mao G, Qu F, Angeli JP, Doll S, Croix CS, Dar HH, Liu B, Tyurin VA, Ritov VB, Kapralov AA, Amoscato AA, Jiang J, Anthonymuthu T, Mohammadyani D, Yang Q, Proneth B, Klein-Seetharaman J, Watkins S, Bahar I, Greenberger J, Mallampalli RK, Stockwell BR, Tyurina YY, Conrad M, Bayir H. Oxidized arachidonic and adrenic PEs navigate cells to ferroptosis. *Nature Chemical Biology,* 13:81-90, 2017

39. Stockwell BR, Friedmann Angeli JP, Bayir H, Bush AI, Conrad M, Dixon SJ, Fulda S, Gascon S, Hatzios SK, Kagan VE, Noel K, Jiang X, Linkermann A, Murphy ME, Overholtzer M, Oyagi A, Pagnussat GC, Park J, Ran Q, Rosenfeld CS, Salnikow K, Tang D, Torti FM, Torti SV, Toyokuni S, Woerpel KA, Zhang DD. Ferroptosis: A regulated cell death nexus linking metabolism, redox biology, and disease. *Cell,* 171:273-285, 2017

40. Fang X, Wang H, Han D, Xie E, Yang X, Wei J, Gu S, Gao F, Zhu N, Yin X, Cheng Q, Zhang P, Dai W, Chen J, Yang F, Yang HT, Linkermann A, Gu W, Min J, Wang F. Ferroptosis as a target for protection against cardiomyopathy. *Proceedings of the Naionall Academy Sciences of United States of America,* 116:2672-2680, 2019

41. Yang WS, SriRamaratnam R, Welsch ME, Shimada K, Skouta R, Viswanathan VS, Cheah JH, Clemons PA, Shamji AF, Clish CB, Brown LM, Girotti AW, Cornish VW, Schreiber SL, and Stockwell BR. Regulation of ferroptotic cancer cell death by GPX4. *Cell,* 156:317-331, 2014

42. Yoshida M, Minagawa S, Araya J, Sakamoto T, Hara H, Tsubouchi K, Hosaka

Y, Ichikawa A, Saito N, Kadota T, Sato N, Kurita Y, Kobayashi K, Ito S, Utsumi H, Wakui H, Numata T, Kaneko Y, Mori S, Asano H, Yamashita M, Odaka M, Morikawa T, Nakayama K, Iwamoto T, Imai H, Kuwano K. Involvement of cigarette smoke-induced epithelial cell ferroptosis in COPD pathogenesis. *Nature Communications,* 10:3145, 2019

43. Takahashi M, Takahashi S, Suzuki C, Jia L, Morimoto H, Ise H, Iwasaki T, Hattori H, Suzuki J, Miyamori I, Kobayashi E, Ikeda U. Interleukin-1beta attenuates beta-very low-density lipoprotein uptake and its receptor expression in vascular smooth muscle cells. *Journal of Molecular Cellular Cardiology,* 38:637-646, 2005
44. Higashi T, Mai Y, Mazaki Y, Horinouchi T, Miwa S. A standardized method for the preparation of a gas phase extract of cigarette smoke. *Biological Pharmaceutical Bulletin,* 39:898-902, 2016
45. Miyoshi H, Blomer U, Takahashi M, Gage FH, Verma IM. Development of a self-inactivating lentivirus vector. *Journal of Virology* 72: 8150-8157, 1998.
46. Kakafika AI, Mikhailidis DP. Smoking and aortic diseases. *Circulation Journal,* 71:1173-1180, 2007
47. Bazzini C, Rossetti V, Civello DA, Sassone F, Vezzoli V, Persani L, Tiberio L, Lanata L, Bagnasco M, Paulmichl M, Meyer G, Garavaglia ML. Short- and long- term effects of cigarette smoke exposure on glutathione homeostasis in human bronchial epithelial cells. *Cellular Physiology and Biochemistry,* 32:129-145, 2013
48. van der Toorn M, Smit-de Vries MP, Slebos DJ, de Bruin HG, Abello N, van Oosterhout AJ, Bischoff R, Kauffman HF. Cigarette smoke irreversibly modifies glutathione in airway epithelial cells. *American Journal of Physiology - Lung Cellular and Molecular Physiology,* 293:L1156-1162, 2007

49. Yang WS, Stockwell BR. Ferroptosis: Death by Lipid Peroxidation. *Trends in Cell Biology,* 26:165-176, 2016

50. Horinouchi T, Higashi T, Mazaki Y, Miwa S. Carbonyl compounds in the gas phase of cigarette mainstream smoke and their pharmacological properties. *Biological Pharmaceutical Bulletin,* 39: 909-914, 2016

51. Kihara T, Yamagishi K, Iso H, Tamakoshi A, Group JS. Passive smoking and mortality from aortic dissection or aneurysm. *Atherosclerosis,* 263:145-150, 2017

52. Nordon IM, Hinchliffe RJ, Loftus IM, Thompson MM. Pathophysiology and epidemiology of abdominal aortic aneurysms. *Nature Reviews Cardiology* 8: 92-102, 2011

53. Norman PE, Curci JA. Understanding the effects of tobacco smoke on the pathogenesis of aortic aneurysm. *Arteriosclerosis, Thrombosis, and Vascular Biology,* 33:1473-1477, 2013

54. Wang Q, Liu Z, Ren J, Morgan S, Assa C, Liu B. Receptor-interacting protein kinase 3 contributes to abdominal aortic aneurysms via smooth muscle cell necrosis and inflammation. *Circulation Research,* 116:600-611, 2015.

55. Park EJ, Park YJ, Lee SJ, Lee K, Yoon C. Whole cigarette smoke condensates induce ferroptosis in human bronchial epithelial cells. *Toxicology Letters,* 303:55-66, 2019

56. Quintana RA, and Taylor WR. Cellular mechanisms of aortic aneurysm formation. *Circulation Research,* 124:607-618, 2019

57. Wen Q, Liu J, Kang R, Zhou B, Tang D. The release and activity of HMGB1 in ferroptosis. *Biochemical Biophysical Research Communications,* 510:278-283, 2019

58. Sakalihasan N, Delvenne P, Nusgens BV, Limet R, Lapiere CM, Activated forms of MMP2 and MMP9 in abdominal aortic aneurysms. *Journal of Vascular Surgery,* 24(1):127-133, 1996

59. Tamarina NA, et al., Expression of matrix metalloproteinases and their inhibitors in aneurysms and normal aorta. *Surgery,*122:264-72, 1997

60. Zilka O, Shah R, Li B, Friedmann Angeli JP, Griesser M, Conrad M, Pratt DA. On the mechanism of cytoprotection by ferrostatin-1 and liproxstatin-1 and the role of lipid peroxidation in gerroptotic cell death. *ACS Central Science,* 3:232-243, 2017

61. Yadav UC, Ramana KV. Regulation of NF-kappaB-induced inflammatory signaling by lipid peroxidation-derived aldehydes. *Oxidative Medicine Cellular Longevity,* 2013:690545, 2013

62. Carnevali S, Petruzzelli S, Longoni B, Vanacore R, Barale R, Cipollini M, Scatena F, Paggiaro P, Celi A, and Giuntini C. Cigarette smoke extract induces oxidative stress and apoptosis in human lung fibroblasts. *American Journal of Physiology - Lung Cellular and Molecular Physiology,* 284:L955–L963, 2003

63. Horiyama S, Takahashi Y, Hatai M, Honda C, Suwa K, Ichikawa A, Yoshikawa N, Nakamura K, Kunitomo M, Date S, Masujima Ts, Takayama M. Methyl vinyl ketone, a toxic ingredient in cigarette smoke extract, modifies glutathione in mouse melanoma cells. Chemical and Pharmaceutical Bulletin (Tokyo), 62(8):772-8, 2014

64. Horiyama Sh, Hatai M, Takahashi Yu, Date S, Masujima Ts, Honda Ch, Ichikawa A, Yoshikawa N, Nakamura K, Kunitomo M, and Takayama M. Intracellular Metabolism of α,β-Unsaturated Carbonyl Compounds, Acrolein, Crotonaldehyde and Methyl Vinyl Ketone, Active Toxicants in Cigarette

Smoke: Participation of Glutathione Conjugation Ability and Aldehyde–Ketone Sensitive Reductase Activity. Chemical Pharmaceutical Bulletin, 64:585–593, 2016

65. Rowe VL, Stevens SL, Reddick TT, Freeman MB, Donnell R, Carroll RC, and Goldman MH, Tenn K. Vascular smooth muscle cell apoptosis in aneurysmal, occlusive, and normal human aortas. Journal of Vascular Surgery, 31(3):567-576, 2000
66. Lopez-Candales A, Holmes DR, Liao S, Scott MJ, Wickline SA, Thompson RW. Decreased vascular smooth muscle cell density in medial degeneration of human abdominal aortic aneurysms. American Journal of Pathology, 150:993-1007, 1997
67. Reilly M, Delanty N, Lawson JA, FitzGerald GA. Modulation of oxidant stress in vivo in chronic cigarette smokers. *Circulation,* 94:19-25, 1996
68. Mezzetti A, Lapenna D, Pierdomenico SD, Calafiore AM, Costantini F, Riario-Sforza G, Imbastaro T, Neri M, Cuccurullo F. Vitamins E, C and lipid peroxidation in plasma and arterial tissue of smokers and non-smokers. *Atherosclerosis* 112:91-99, 1995
69. Yang HL, Korivi M, Chen CH, Peng WJ, Chen CS, Li ML, Hsu LS, Liao JW, Hseu YC. Antrodia camphorata attenuates cigarette smoke-induced ROS production, DNA damage, apoptosis, and inflammation in vascular smooth muscle cells, and atherosclerosis in ApoE-deficient mice. *Environmental Toxicology,* 32:2070-2084, 2017
70. Yamaguchi Y, Matsuno S, Kagota S, Haginaka J, and Kunitomo M. Oxidants in cigarette smoke extract modify low-density lipoprotein in the plasma and facilitate atherogenesis in the aorta of Watanabe heritable hyperlipidemic rabbits. *Atherosclerosis,* 156:109-117, 2001

71. Hinman A, Holst CR, Latham JC, Bruegger JJ, Ulas G, McCusker KP, Amagata A, Davis D, Hoff KG, Kahn-Kirby AH, Kim V, Kosaka Y, Lee E, Malone SA, Mei JJ, Richards SJ, Rivera V, Miller G, Trimmer JK, Shrader WD. Vitamin E hydroquinone is an endogenous regulator of ferroptosis via redox control of 15-lipoxygenase. *PLoS One,* 13:e0201369, 2018
72. Sawada H, Hao H, Naito Y, Oboshi M, Hirotani S, Mitsuno M, Miyamoto Y, Hirota S, Masuyama T. Aortic iron overload with oxidative stress and inflammation in human and murine abdominal aortic aneurysm. *Arteriosclerosis, Thrombosis, and Vascular Biology,* 35:1507-1514, 2015
73. Feng H, Stockwell BR. Unsolved mysteries: How does lipid peroxidation cause ferroptosis? *PLoS Biol,* 16:e2006203, 2018
74. Franco R, Cidlowski JA. Glutathione efflux and cell death. *Antioxid Redox Signal,* 17:1694-1713, 2012
75. Mari M, Morales A, Colell A, Garcia-Ruiz C, Fernandez-Checa JC. Mitochondrial glutathione, a key survival antioxidant. *Antioxidants and Redox Signaling,* 11: 2685-2700, 2009
76. Gao M, Yi J, Zhu J, Minikes AM, Monian P, Thompson CB, Jiang X. Role of mitochondria in ferroptosis. *Molecular Cell,* 73:354-363, 2019